NASA TECHNICAL REPORT

NASA TR R-300

AERODYNAMIC FORCES ON A STATIONARY AND OSCILLATING CIRCULAR CYLINDER AT HIGH REYNOLDS NUMBERS

by

George W. Jones, Jr.
Langley Research Center

Joseph J. Cincotta
The Martin Company

and

Robert W. Walker
George C. Marshall Space Flight Center

NATIONAL AERONAUTICS AND SPACE ADMINISTRATION • WASHINGTON, D. C. • FEBRUARY 1969

AERODYNAMIC FORCES ON A STATIONARY AND OSCILLATING CIRCULAR CYLINDER AT HIGH REYNOLDS NUMBERS

By George W. Jones, Jr.
Langley Research Center
Langley Station, Hampton, Va.

Joseph J. Cincotta
The Martin Company
Baltimore, Md.

and Robert W. Walker
George C. Marshall Space Flight Center
Huntsville, Ala.

NATIONAL AERONAUTICS AND SPACE ADMINISTRATION

For sale by the Clearinghouse for Federal Scientific and Technical Information
Springfield, Virginia 22151 – CFSTI price $3.00

CONTENTS

	Page
SUMMARY	1
INTRODUCTION	2
SYMBOLS	3
APPARATUS AND TESTS	7
Test Facility	7
Model	7
Instrumentation and Data-Reduction Procedures	10
Tests	11
RESULTS AND DISCUSSION	12
Static Measurements	12
Static pressures	12
Drag data	17
Characteristics of Unsteady Lift Measured on Stationary Cylinder	26
Frequency content of unsteady lift	26
Magnitude of unsteady lift	30
Measurement of Unsteady Lift Due to Cylinder Motion	33
Power spectral density and root-mean-square values	33
Lift-force vector at frequency of cylinder oscillation	36
Aerodynamic derivatives of lift due to motion	36
CONCLUSIONS	43
APPENDIX A – ESTIMATION OF SOLID-BLOCKAGE INTERFERENCE	45
APPENDIX B – DETAILS OF INSTRUMENTATION AND DATA-REDUCTION PROCEDURES	46
REFERENCES	53
TABLES	55

AERODYNAMIC FORCES ON A STATIONARY AND OSCILLATING CIRCULAR CYLINDER AT HIGH REYNOLDS NUMBERS

By George W. Jones, Jr., Joseph J. Cincotta, and Robert W. Walker

SUMMARY

A wind-tunnel investigation has been made of the steady drag and unsteady lift (lateral) forces on a stationary and oscillating circular cylinder in two-dimensional flow at Reynolds numbers from 0.36×10^6 to 18.70×10^6 and at Mach numbers M up to 0.6. The experimental data were obtained in the Langley transonic dynamics tunnel from tests of a 3-foot (0.914-meter) diameter cylinder instrumented to measure directly the unsteady lift and mean drag forces on the cylinder. The cylinder could be held fixed or oscillated laterally to the flow at frequencies from 3 to 20 hertz. The results of the investigation verified and considerably extended the range of previous knowledge in this area.

For the stationary cylinder, the most important results may be summarized as follows: The static-pressure distributions, the mean drag coefficients at $M \leq 0.2$, and the Strouhal number of the unsteady lift forces follow the trends established by previous investigators up to the limits of Reynolds number investigated. At higher (hitherto unexplored) Reynolds numbers, each of these parameters remains essentially constant; that is, the static-pressure distribution remains essentially the same above a Reynolds number of 8×10^6, the mean drag coefficient is approximately 0.54, and the Strouhal number is approximately 0.3. The unsteady lift force can be categorized into three regimes dependent upon Reynolds number – wide-band random, narrow-band random, and quasi-periodic. The root-mean-square unsteady lift coefficient at Mach numbers less than 0.3 varies over a wide range at Reynolds numbers from 1.4×10^6 to 8×10^6; then, at higher Reynolds numbers, it is a single-valued function which decreases with increasing Reynolds number.

For the oscillating cylinder, the most important results may be summarized as follows: Oscillation of the cylinder in the lift direction has no significant effect on the mean drag coefficient. An unsteady lift due to cylinder motion, which increases with amplitude of motion, exists only when the cylinder is oscillated at or relatively near the aerodynamic Strouhal frequency for the stationary cylinder. This unsteady lift is a negative (destabilizing) aerodynamic damping force at cylinder frequencies below the stationary-cylinder Strouhal frequency. As the cylinder frequency is increased through and above the Strouhal frequency, there is an abrupt change in the unsteady lift due to motion to a positive (stabilizing) aerodynamic damping force. Aerodynamic derivatives with respect to displacement of the components of unsteady lift due to motion decrease nonlinearly with increasing amplitude of motion.

INTRODUCTION

The aerodynamic forces produced by flow about circular cylinders with the longitudinal axis perpendicular to the flow have been of interest since the ancient invention of the Aeolian harp. For some time it has been generally known that the behavior of a cylinder in a laminar flow at low Reynolds numbers is characterized by the formation of a Kármán vortex street in which the periodic separation of continuous vortices along alternate sides of the cylinder gives rise to periodic forces in the lift (lateral) direction. Recently, the response to ground winds of large flexible structures, such as metal smokestacks and cylindrical space vehicles standing on the launch pad, has led to considerable interest in the spontaneously generated unsteady aerodynamic forces on circular cylinders at high Reynolds numbers. These unsteady forces are produced by vortices shed alternately from the sides of the structure and by atmospheric turbulence. For lightly damped structures, these forces are capable of exciting large-amplitude vibratory response. The unsteady forces associated with vortex shedding are not well understood or amenable to analysis. Many investigators have made experimental studies, such as those given in references 1 to 11, which have given some understanding of the mechanism of vortex shedding, particularly at lower Reynolds numbers. However, at higher Reynolds numbers, there is little information on the nature of these aerodynamic forces. In particular, the question of how these forces are affected by the motion of the structure as it deflects in response to the aerodynamic loads has needed investigation.

A wind-tunnel investigation has, therefore, been conducted on a large circular cylinder in a two-dimensional flow at Reynolds numbers from 0.36×10^6 to 18.70×10^6. The cylinder was instrumented so that the mean drag and the unsteady lift forces could be read directly. In addition to being held stationary, the cylinder could be oscillated over a range of amplitudes and frequencies. This oscillation capability was used to investigate the effects of cylinder motion on the aerodynamic forces generated. On the stationary cylinder, static-pressure distributions were measured (at one longitudinal station) throughout the test Reynolds number range, and flow visualization techniques were used to gain additional understanding of the flow field about the cylinder. Figure 1 presents a comparison of the Reynolds number and nondimensional-frequency-of-oscillation ranges of this investigation with those of previous investigations. This figure shows that this investigation has greatly extended the Reynolds number and nondimensional-frequency-of-oscillation ranges over which the aerodynamic forces on cylinders have been studied.

The investigation was a joint effort by the National Aeronautics and Space Administration (George C. Marshall Space Flight Center and Langley Research Center) and The Martin Company, Baltimore. The Martin Company, under contract, supplied the model and participated in the tests and in some of the data reduction. The results of the investigation are presented and analyzed herein.

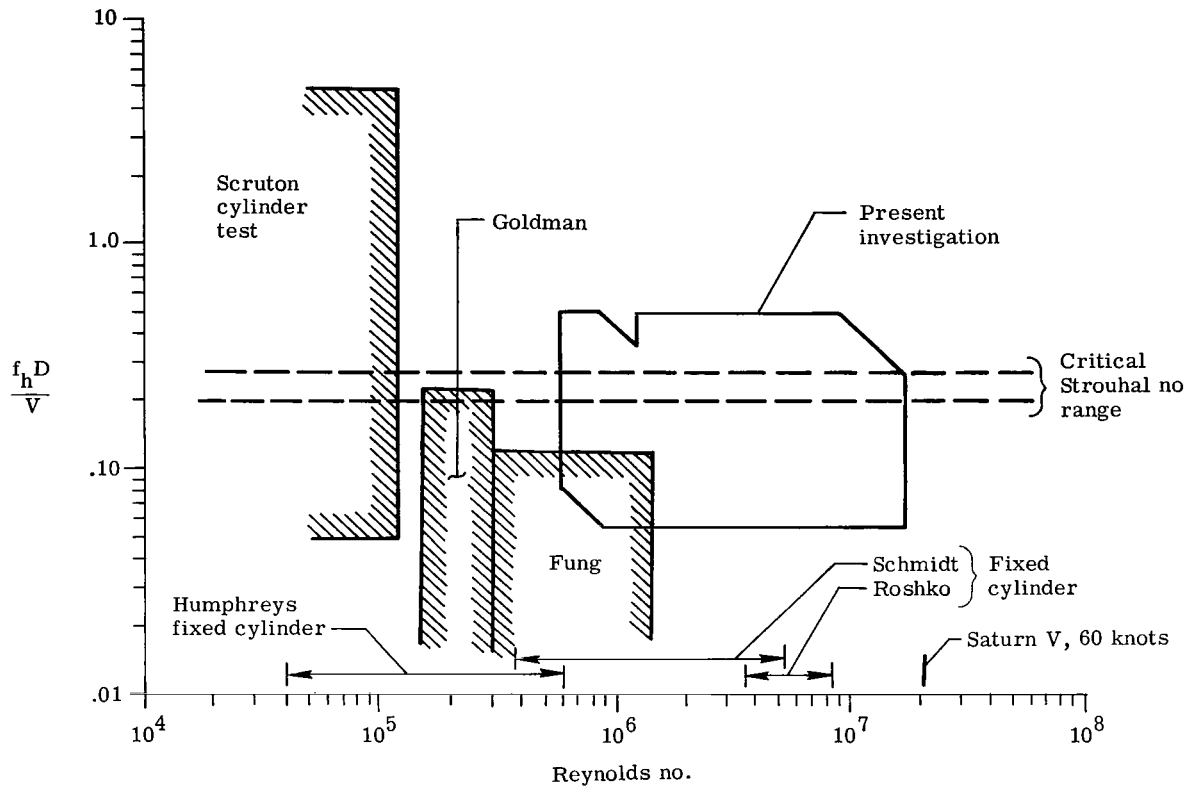

Figure 1.- Comparison of R_N and $\frac{f_h D}{V}$ ranges of present investigation with previous investigations (refs. 1 to 5, 7, and 8).

SYMBOLS

[The words "instrumented section" used in defining symbols refer to the large instrumented model section having a length of 2.33 diameters]

A projected area of instrumented section of cylinder

C_D mean drag coefficient for instrumented section of cylinder

$|C_L|$ absolute value of aerodynamic-lift-coefficient vector at frequency of oscillation of cylinder, $|C_{L,Re} + iC_{L,Im}|$

$C_{L,Im}$ imaginary component (in phase with cylinder velocity) of aerodynamic-lift-coefficient vector at frequency of oscillation of cylinder

$C_{L,Re}$ real component (in phase with cylinder displacement) of aerodynamic-lift-coefficient vector at frequency of oscillation of cylinder

$C_{L,rms(h/D)}$ root-mean-square value of unsteady lift coefficient on instrumented section of oscillating cylinder

$C_{L,rms(0)}$ root-mean-square value of unsteady lift coefficient on instrumented section of stationary cylinder

c_d section mean drag coefficient for stationary cylinder

c_l section mean lift coefficient for stationary cylinder

c_p section static-pressure coefficient on stationary cylinder, $\Delta p/q$

$c_{p,base}$ average of section pressure coefficients at rear of cylinder between $\phi = 150^o$ and $\phi = 210^o$

D diameter of test cylinder, 3 feet (0.914 meter)

F_{Bottom} sum of lift forces at bottom of instrumented section of cylinder, $F_{L,3} + F_{L,4}$

F_D total drag force on instrumented section of cylinder, $F_{D,1} + F_{D,2}$

$F_{D,1}$, $F_{D,2}$ forces in drag direction on instrumented section of cylinder measured by drag transducers 1 and 2, respectively

F_L total aerodynamic lift force on instrumented section of cylinder, $F_{Top} + F_{Bottom} - F_{\ddot{x}}$

$\overline{F}_L$ mean value of F_L

$F_{L,Im}$ imaginary component (in phase with velocity) of unsteady lift force on instrumented section of cylinder at frequency of oscillation of cylinder

$F_{L,Re}$ real component (in phase with cylinder displacement) of unsteady lift force on instrumented section of cylinder at frequency of oscillation of cylinder

$F_{L,1}$, $F_{L,2}$, $F_{L,3}$, $F_{L,4}$ — forces in lift direction on instrumented section of cylinder measured by lift transducers 1, 2, 3, and 4, respectively

F_{Top} — sum of lift forces at top of instrumented section of cylinder, $F_{L,1} + F_{L,2}$

$F_{\ddot{x}}$ — inertia force in lift direction on instrumented section of cylinder

f — frequency

f_h — forcing frequency of oscillation of cylinder

f_s — vortex-shedding frequency of cylinder, defined as predominant frequency of autocorrelation function of unsteady-lift-data sample

f_1 — fundamental frequency of model cylinder (which had adjustable natural frequencies)

g — acceleration due to gravity

h — instantaneous amplitude of cylinder displacement under forced oscillation, $h_0 \cos \omega t$

h_a — Scruton-type aerodynamic derivative (see ref. 4) of real component of unsteady-aerodynamic-lift-coefficient vector at frequency of oscillation of cylinder, $-\frac{C_{L,Re}}{2S^2(h/D)}$

h_0 — amplitude (0-peak) of cylinder displacement

$(h_0/D)_{rms}$ — root-mean-square value of h_0/D

k_a — Scruton-type aerodynamic derivative of imaginary component of unsteady-aerodynamic-lift-coefficient vector at frequency of oscillation of cylinder $-\frac{C_{L,Im}}{4\pi S^2(h/D)}$

M — Mach number

$p(F_L)$ — probability density function of unsteady lift force

q	free-stream dynamic pressure, $\frac{1}{2}\rho V^2$
R_N	Reynolds number based on cylinder cross-section diameter, $\frac{\rho VD}{\mu}$
$R(\tau)$	autocorrelation function of unsteady lift force
S	aerodynamic Strouhal number, $\frac{f_S D}{V}$
T	integration time constant used in data reduction
T_{F_L}	total amount of time that F_L falls inside range $\left(F_L, F_L + \Delta F_L\right)$ during time period T
t	time
V	velocity of test medium
$\bar{v}$	mean value of perturbation velocity in measuring turbulence level of tunnel flow
$\ddot{x}$	acceleration in lift direction of instrumented section of cylinder
Δp	local-surface static pressure minus free-stream static pressure
ΔS	half-power Strouhal bandwidth of unsteady lift
θ	phase angle between cylinder displacement and unsteady lift force due to motion of cylinder at frequency of oscillation of cylinder
μ	dynamic viscosity of test medium
ρ	density of test medium
τ	time displacement variable of autocorrelation function
ϕ	angular location of static-pressure orifice with respect to direction of free-stream flow

$\Phi_{C_L}\left(\frac{fD}{V}\right)$ power spectral density of unsteady aerodynamic lift coefficient as function of $\frac{fD}{V}$, $\left(F_L\right)^2 = (qA)^2 \int_0^\infty \Phi_{C_L}\left(\frac{fD}{V}\right) d\left(\frac{fD}{V}\right)$

ω circular frequency

APPARATUS AND TESTS

Test Facility

The Langley transonic dynamics tunnel used for the investigation is a single-return-flow, variable-pressure, slotted-throat wind tunnel with a test section 16 feet (4.877 m) square (having cropped corners). The tunnel can operate at stagnation pressures from about 0.05 atmospheric to slightly above atmospheric at Mach numbers from 0 to 1.2. Either air or freon gas may be used as the test medium. This facility is particularly suited for general dynamics testing because Mach number and Reynolds number can be varied independently and are continuously controllable. The flow in the test section for the ranges of this investigation had a maximum deviation from average free-stream Mach number of approximately 0.003 and was moderately turbulent, having a turbulence level of $\left(\sqrt{\bar{v}^2}/V\right) \approx 0.0017$. Although the model cross-sectional area appears large in relation to the tunnel cross-sectional area, as shown in figure 2, the estimated solid-blockage interference was negligible (see appendix A), and no wall-interference corrections have been made to the data.

Model

The cylinder model had a 3-foot (0.914-meter) diameter and spanned the tunnel from floor to ceiling with its longitudinal axis perpendicular to the tunnel flow and centered in the test-section span. The model structure consisted of an inner supporting cylinder, an outer cylinder divided into sections, a variable-stiffness suspension system, and a hydraulic shaker system. A photograph of the model installed in the tunnel is given in figure 2 and assembly details are shown in figure 3. The four principal parts of the model structure are discussed in the following paragraphs.

The inner cylinder was a seamless aluminum tube, 17 feet (5.182 meters) long and 19 inches (0.483 meter) in diameter, which extended through openings in the floor and ceiling of the test section. This cylinder provided the necessary load carrying capability to withstand the inertia and aerodynamic loads imposed on the outer cylinder during the tests. Four adjustable rings were attached to the inner cylinder, one at each end of the outer-cylinder top and bottom sections (see fig. 3). These rings provided small spanwise adjustments to the outer sections.

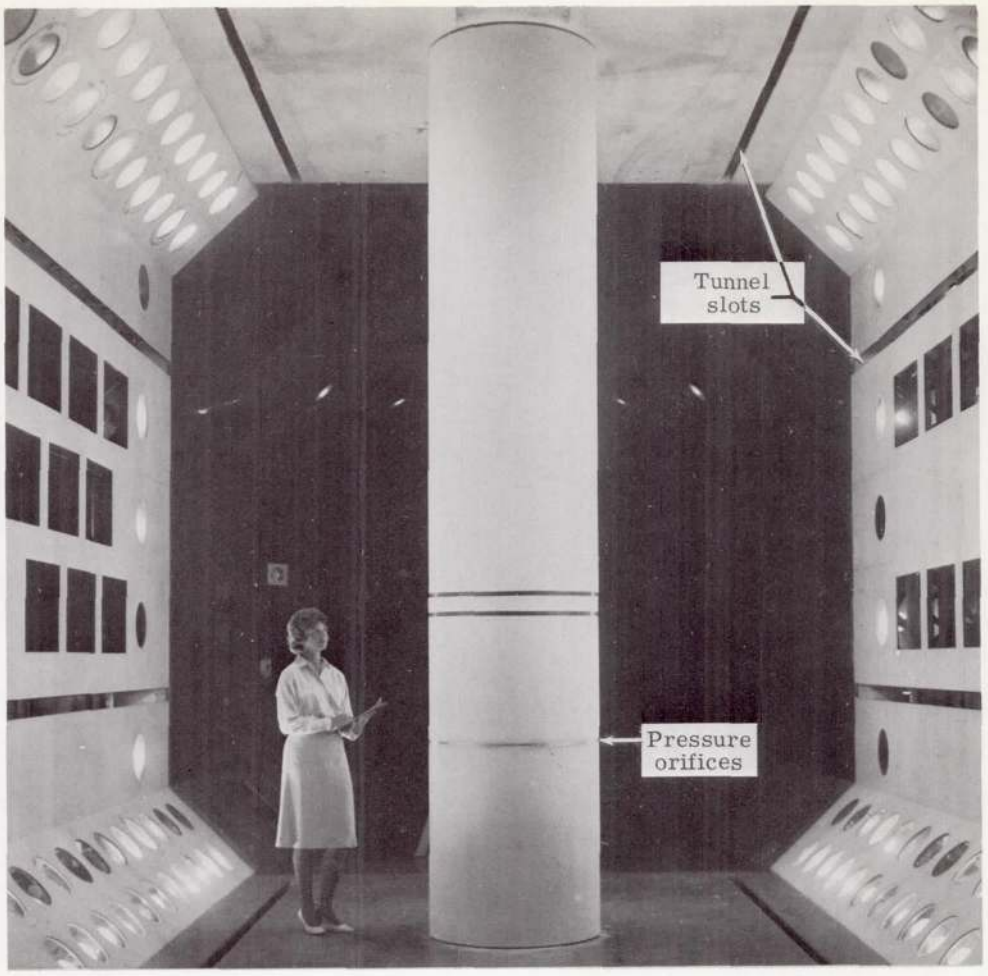

Figure 2.- Cylinder model installed in the wind tunnel. L-2996-2

The outer cylinder consisted of four cylindrical sections. These sections were of lightweight-aluminum, honeycomb-skin-sandwich construction with an outer diameter of 3 feet (0.914 meter) and spanwise (longitudinal) lengths of 1.0D, 2.33D, 0.1D, and 1.9D. The 1.0D and 1.9D sections were not instrumented and were attached rigidly to each end of the inner support cylinder (adjacent to the test-section floor and ceiling) by the adjustable rings previously described. The 2.33D and 0.1D sections were instrumented for the test program (although, as explained subsequently, the data from the 0.1D section are not presented) and were attached to the inner support cylinder by force transducers oriented to read forces in the lift and drag directions. The force transducers were linked to a system of flexures and antirotation rings (see figs. 3 and 4) which permitted translation, but not rotation, of the outer cylinder section in the lift and drag directions. Thus, the cross-axis signals between the lift and drag force transducers were minimized. The instrumented sections were of continuous-type construction to minimize flow disturbance.

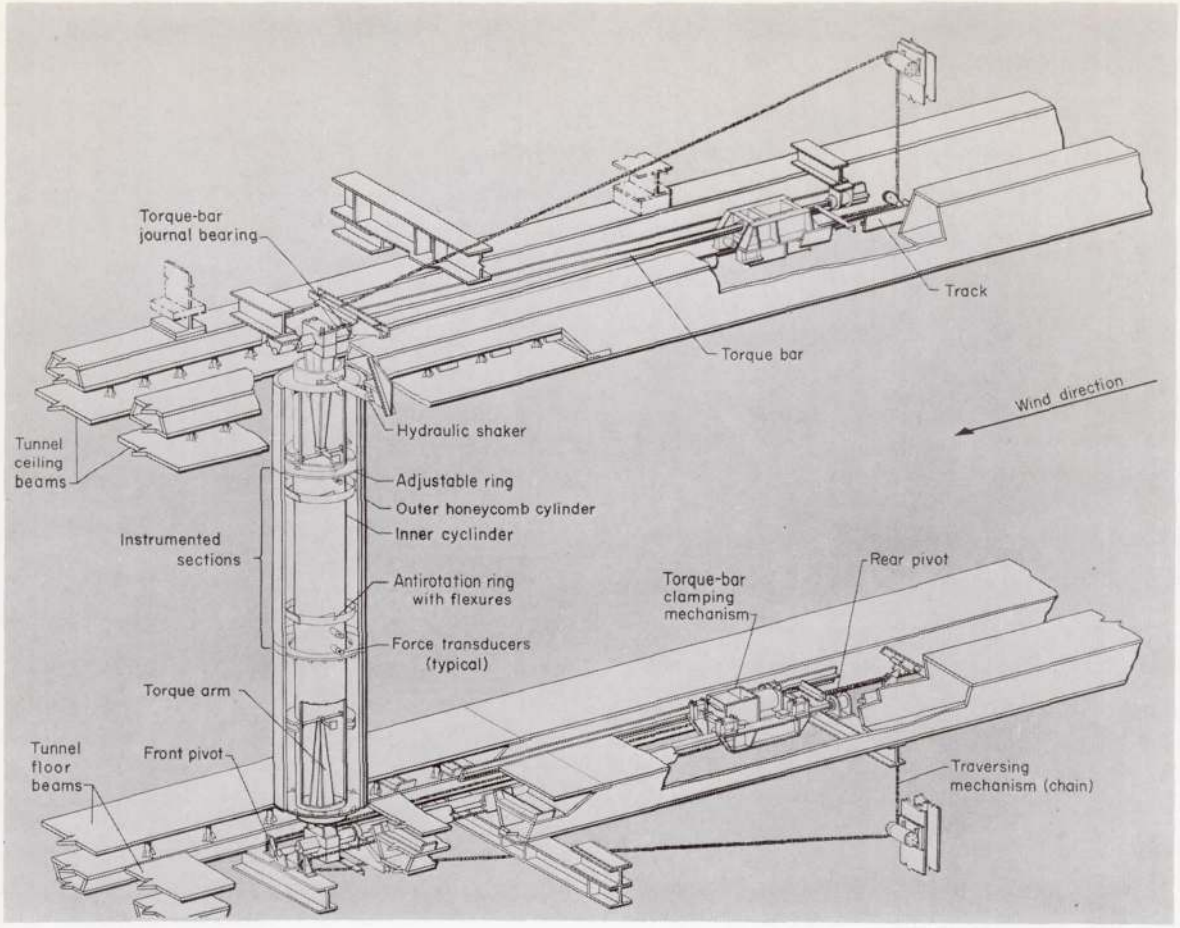

Figure 3.- Model assembly and installation details.

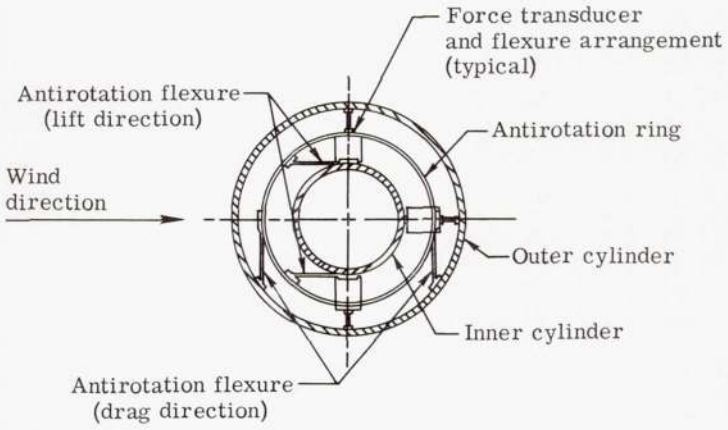

Figure 4.- Application of flexures on antirotation ring and force transducers.

The three circumferential gaps between adjacent outer cylinder sections were held to 0.03 inch (0.762 mm) and were originally designed with a simple labyrinth seal to prevent flow from penetrating the gaps. In practice, the gaps and seal as designed created unsatisfactory flow disturbances and the gaps were then filled with a silicone rubber compound. This flexible rubber seal effectively eliminated the flow disturbances but allowed small relative motion between adjacent cylinder sections. The seal transmitted in shear to the 0.1D section only about 1 percent of the load on the 2.33D instrumented section.

The model suspension system consisted of two identical assemblies, one located at each end of the inner cylinder and mounted outside the tunnel test section (see fig. 3). The basic parts of each suspension assembly were a torque bar, a remotely operated torque-bar clamping mechanism, and a torque arm which connected the inner cylinder to the torque bar. The torque arms (which were pin-connected to the inner cylinder at a location 3 feet (0.914 meter) inside the inner cylinder) allowed lateral translation of the model. Torque loads produced in the torque bars by this model motion were transferred to the torque-bar clamping mechanisms which, in turn, transferred the loads into the tunnel structural beams. The system was designed to withstand loads up to 60g; however, the actual loads did not exceed 30g.

The cylinder model and torque-bar suspension assembly formed a resonant system in the cylinder translatory mode. The natural frequencies of the system could be varied by moving the clamping mechanisms along the torque bar and reclamping; the effective length of the torque bars was changed in this manner. The system could be tuned between 3 and 20 hertz so that the force required to drive the model in the translatory mode at any desired frequency in this range was minimized. This force was supplied by the hydraulic shaker system, which had one shaker attached to each end of the inner cylinder. Each of these two shakers was capable of providing a force up to 1400 pounds (6227 newtons) at 3 inches (7.62 cm) maximum amplitude, and the system could control the amplitude throughout a frequency range from 3 to 20 hertz. The shakers were controlled from a single console to obtain synchronized amplitude at each shaker head.

Vibration tests were conducted to determine the elastic resonant frequencies of the model assembly. These tests showed that the natural frequencies of the model were well above the range of interest of the test data, with the lowest value being 70 hertz.

Instrumentation and Data-Reduction Procedures

A Martin-developed instrumentation system called the Inertia Compensated Balance (ICB) was used to measure directly on the stationary or oscillated cylinder the unsteady aerodynamic lift force on the 2.33D-length instrumented outer-cylinder section. This ICB system electrically combined the signals from the lift strain-gage force transducers with the signals from a strategically located accelerometer in such a manner as to cancel

out the forces due to inertia and give a direct measure of the unsteady aerodynamic lift force. Although it was initially planned to measure the unsteady drag force in a similar manner, a failure of the drag ICB system (unrepairable in the time available) during model checkout prevented such measurements. However, measurements of the mean drag on the large instrumented outer-cylinder section were obtained from the drag transducers. A single row of static-pressure orifices measured the static-pressure distribution around the cylinder at one longitudinal station, 1.14 diameters from the lower end of the outer cylinder. An oil-film technique described in reference 12 was used to obtain photographic and eye-witness visualization of the mean flow on the cylinder surface.

A number of data-reduction procedures, both "on-line" and "after-the-fact," were used to analyze the data, particularly the unsteady lift-force data on the stationary and oscillating cylinder. The mean square value, the power spectral density, the autocorrelation function, and the probability density were obtained in addition to time-history samples of the lift force. Also, for the oscillating cylinder, the unsteady lift force was resolved by means of an analog computer into its components in phase and 90° out of phase with displacement.

A more detailed description of the instrumentation and the data-reduction procedures used to analyze the signals from the instrumentation is presented in appendix B. This appendix gives instrumentation block diagrams and presents a discussion of the equipment techniques, the analysis parameters, and the relative accuracies for the data-reduction procedures.

Tests

During the test program, the mean drag and unsteady lift forces were measured at Reynolds numbers from 0.36×10^6 to 18.70×10^6 at Mach numbers up to 0.6 with the cylinder held stationary and with the cylinder oscillated at model reduced frequencies $f_h D/V$ from 0.06 to 0.50. Static pressures were measured only with the cylinder held stationary. The use of air and freon test mediums at various densities gave a broad range of Reynolds number and allowed a separate investigation of Mach number and Reynolds number effects on the aerodynamic force measurements.

The test program was accomplished in two phases. In the first phase, measurements were made of the static pressures, unsteady lift, and mean drag with the cylinder held stationary in the flow. During this phase, the flow in the vicinity of the three 0.03-inch (0.762-mm) gaps between the fixed and instrumented cylinder sections was seriously disturbed, even though the gaps were equipped with a labyrinth seal. After a period of experimentation, an additional sealing of the gaps with a silicone rubber compound was found to essentially eliminate the disturbance. Because of this gap effect, except for sufficient drag data to illustrate the problem, only the static-pressure data

are presented from this phase of the program. In the second phase of the tests, with the gaps sealed with silicone rubber, measurements were made of the unsteady lift and mean drag forces, both with the cylinder held fixed and with the cylinder oscillating laterally over a range of frequencies and amplitudes. Before starting this phase of the tests, the flexible tubing between the static-pressure orifices and the manometer board was removed in order to permit the cylinder to be oscillated. Consequently, no static-pressure measurements were taken with the gaps sealed with silicone rubber.

The procedures used in measuring the static pressures and the unsteady lift and mean drag forces were as follows: For static-pressure measurements, a desired wind-tunnel test condition was established and held constant until the manometer board stabilized and a photograph was taken of the manometer board. For measurement of the unsteady lift and steady drag aerodynamic forces, a desired test condition was established and held constant while a 1- to 2-minute data sample was recorded and an "on-line" analysis was made.

RESULTS AND DISCUSSION

The results and discussion are organized so that static data such as pressure distributions and mean drag are presented first. These data are accompanied by remarks about flow conditions observed during the tests. After these data have been discussed, the unsteady lift on the stationary cylinder and the unsteady lift due to cylinder motion are presented.

Static Measurements

Static pressures.- Static-pressure distributions were measured at one longitudinal station, 1.14 diameters above the floor of the test section, by using 48 static-pressure orifices spaced around the periphery of the cylinder. The pressure distributions were measured on the stationary cylinder at Reynolds numbers from 0.36×10^6 to 18.70×10^6 at Mach numbers from 0.05 to 0.46. Figure 5 presents, in order of increasing Reynolds number, nine selected pressure distributions. For static-pressure distributions at Reynolds numbers less than about 0.75×10^6, difficulty was experienced in holding a steady tunnel velocity; therefore, measurements of the tunnel flow parameters and the static-pressure distributions are subject to inaccuracies not found at Reynolds numbers above about 0.75×10^6.

The pressure distributions at Reynolds numbers from 0.52×10^6 to 1.31×10^6 (figs. 5(a) and 5(b)) show bulges at $\phi \approx 100^\circ$ and $\phi \approx 260^\circ$. These bulges are believed to be evidence of the occurrence of laminar separation bubbles. As discussed in reference 13, at very low Reynolds numbers, the flow on a cylinder is laminar with a laminar

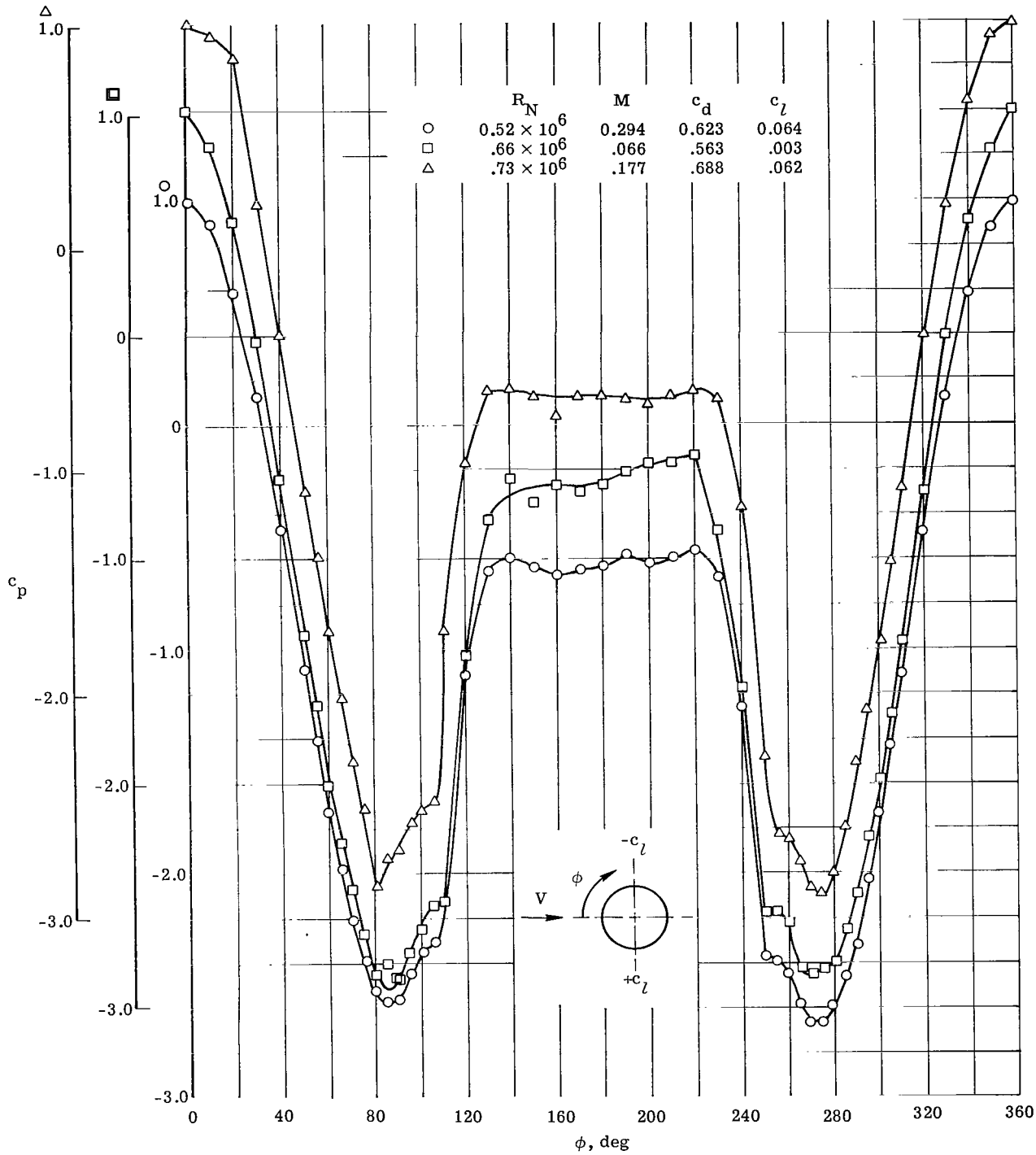

(a) Pressure distributions at Reynolds numbers from 0.52×10^6 to 0.73×10^6.

Figure 5.- Selected pressure distributions measured around circumference of cylinder at one longitudinal station and at several Reynolds numbers.

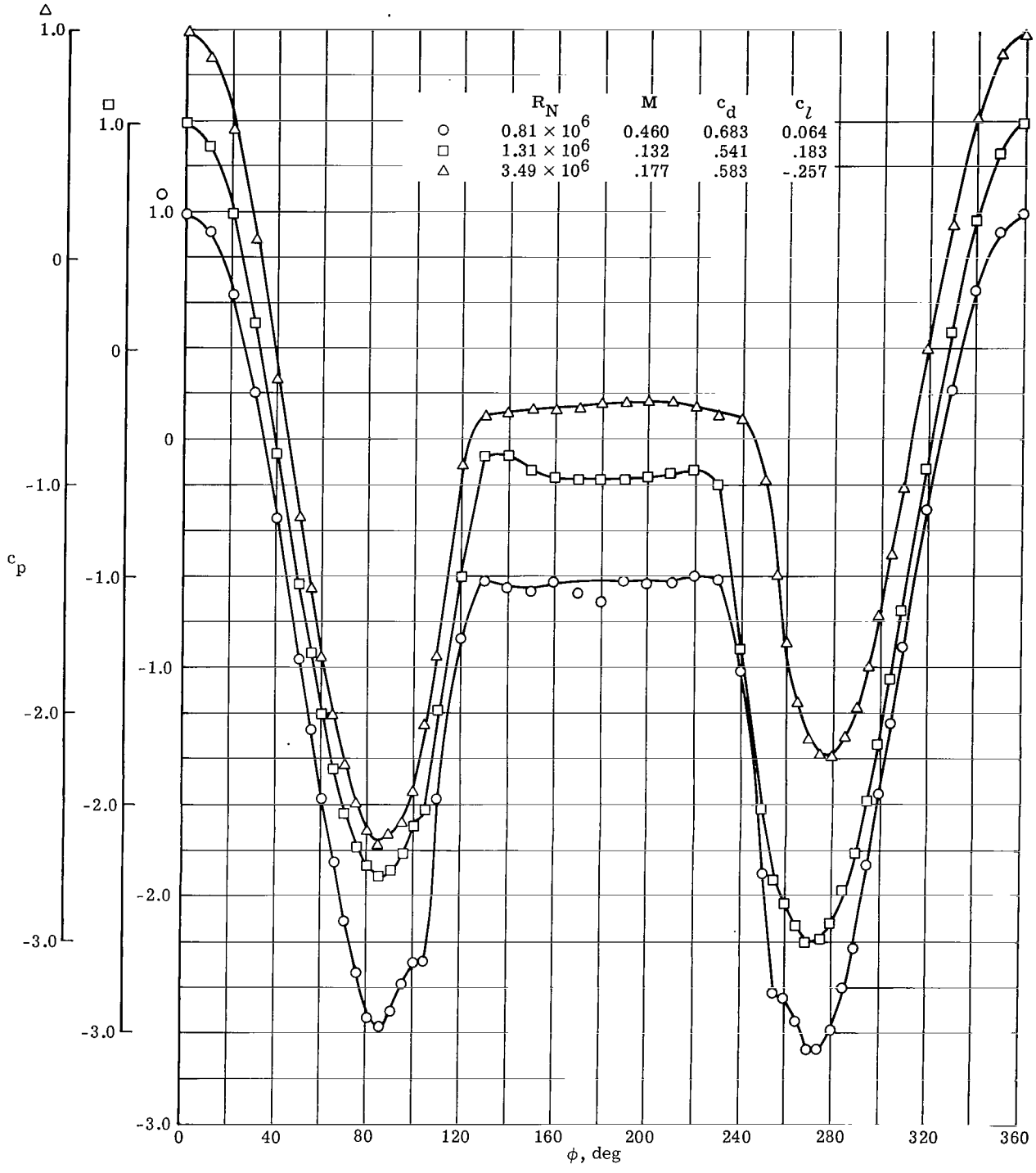

(b) Pressure distributions at Reynolds numbers from 0.81 × 10^6 to 3.49 × 10^6.

Figure 5.- Continued.

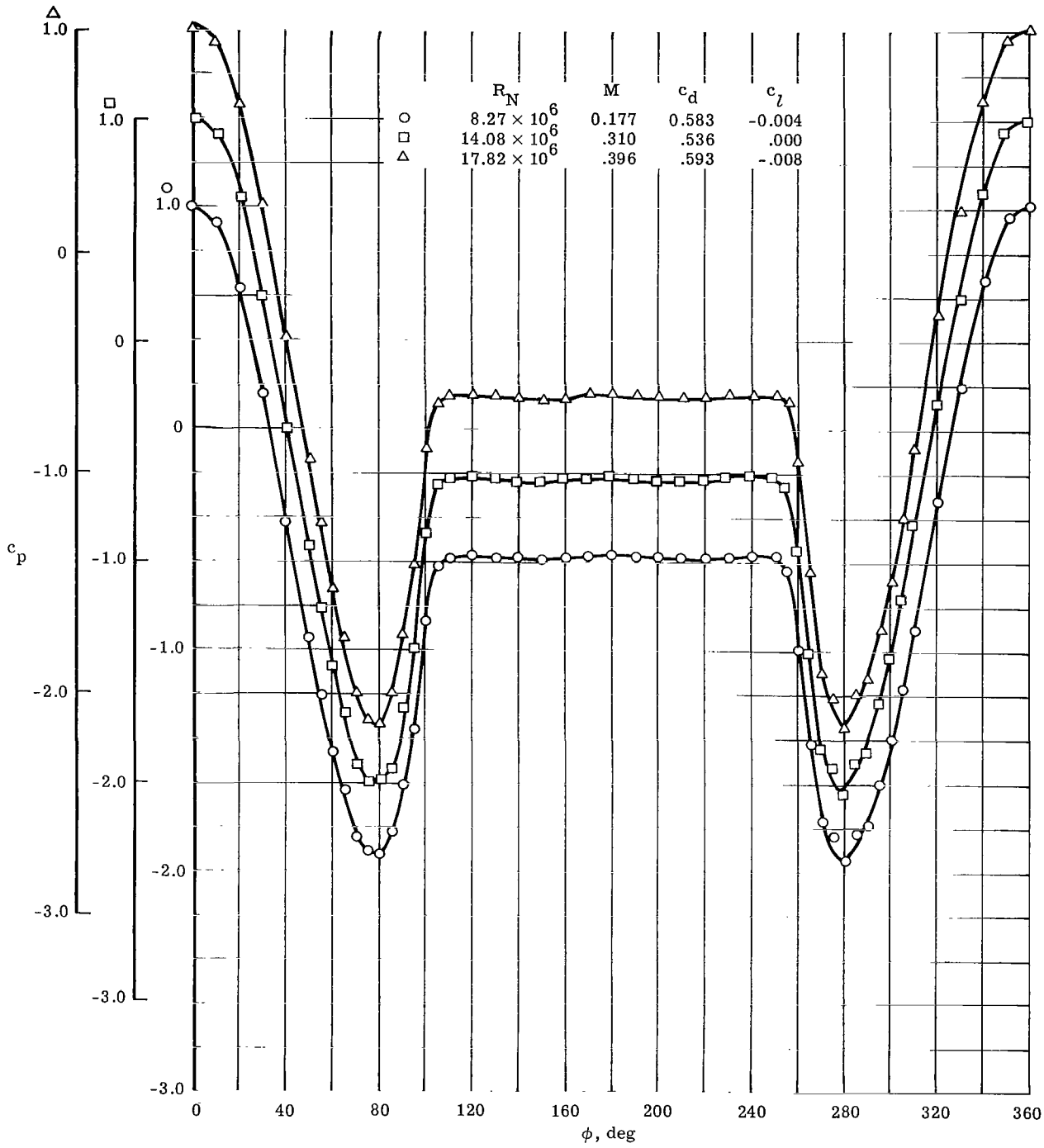

(c) Pressure distributions at Reynolds numbers from 8.27×10^6 to 17.82×10^6.

Figure 5.- Concluded.

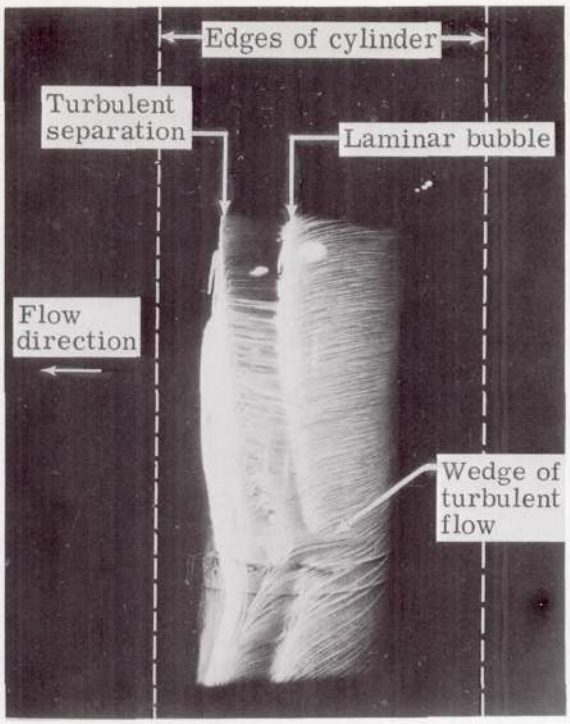

L-68-10,013

Figure 6.- Oil-flow photograph depicting a laminar separation bubble at Reynolds number of 1.73×10^6.

separation. At higher Reynolds number, the separated laminar boundary layer undergoes transition and reattaches to form a laminar separation bubble after which the turbulent flow separates at some point downstream. Figure 6 shows a visualization of a typical laminar separation bubble on the cylinder obtained by the oil-film technique described in reference 12. The laminar bubble and the downstream turbulent separation lines are clearly discernible (the white vertical dashed lines represent the edges of the cylinder). As Reynolds number increases further, the size of the bubble decreases until the transition to turbulent flow moves upstream of the laminar separation location, and the bubble disappears. The static-pressure distributions (fig. 5) exhibited the characteristic bulges at Reynolds numbers up to 1.31×10^6.

The static-pressure distributions at $R_N = 1.31 \times 10^6$ and $R_N = 3.49 \times 10^6$ in figure 5(b) show unsymmetrical negative pressure dips on the symmetric cylinder at $\phi \approx 80^o$ and $\phi \approx 280^o$. As might be expected, integration of these static-pressure distributions indicates a definite value of section lift. Table I(c) and the tables inserted in figure 5 give the values of the section lift and drag coefficients obtained from the integrated values of the static-pressure distributions in the lift and drag directions.

A probable cause for the asymmetry in the flow (as indicated by the substantial values of c_l in the tables) is shown in figure 6. Note the wedge of turbulent flow on the lower central portion of the cylinder. This flow wipes out the laminar separation bubble, as evidenced by the single separation line that bulges forward of the turbulent separation line. If a wedge of turbulent flow that changes the separation line occurred on only one side of the cylinder, the resulting pressure distribution would be unsymmetrical and thus generates a lift force. Such wedges of turbulent flow were a frequent occurrence at Reynolds numbers below about 6×10^6 where the flow was either laminar or mixed laminar and turbulent. The wedges could be traced to specks of dirt or small scratches on the surface and they occurred even though care was taken in manufacturing a truly circular and smooth cylinder. The out-of-roundness was held to ±0.015 inch (±0.381 mm) in diameter, and the waviness of the surface was held to ±0.0001 inch (±0.00254 mm). Thus, at Reynolds numbers below about 6×10^6 where the flow is completely or partly laminar,

flow disturbances will be triggered, even on a polished round cylinder, by specks of dirt or small scratches on the surface. These disturbances, if asymmetric, produce a mean lift force.

At Reynolds numbers greater than about 6×10^6, the turbulent transition has moved upstream until the flow about the cylinder is predominantly or fully turbulent. The turbulent flow is not as easily disturbed as the laminar flow or the flow with a laminar separation bubble. The pressure distributions at Reynolds numbers from 8.27×10^6 to 17.82×10^6 of figure 5(c) are in this predominantly turbulent flow Reynolds number range. These distributions are much more symmetrical than those at Reynolds numbers below 6×10^6 and the section-lift-coefficient values are negligible. In the hitherto unexplored Reynolds number range from 8.27×10^6 to 18.70×10^6, increasing Reynolds number had little effect on the distribution of pressure except for a slight increase in the negative pressure peaks.

Drag data.- The mean drag was obtained on the 2.33D-length instrumented section of the cylinder over a Reynolds number range from 0.36×10^6 to 18.27×10^6. Both air and freon test mediums were used at atmospheric and reduced pressures to obtain these data. Initially, a secondary objective of this study was to measure fluctuating drag forces in addition to measurements of fluctuating lift forces. Accordingly, the model was equipped to measure unsteady drag on the 0.1D section by using the Inertia Compensated Balance (ICB) system. Unfortunately, because of the previously discussed failure of the drag component of this system, no measurements were made of the unsteady drag force and only the mean drag force was measured. All subsequent references to drag data in this paper are for the measured mean drag force. Fortunately, the unsteady portion of the drag force is known to be much smaller than the unsteady lift force. (For example, see ref. 2.)

In the initial phase of the investigation, as previously mentioned, extensive aerodynamic disturbances were found to be caused by the gaps between the instrumented and fixed outer-cylinder sections, even though these gaps were closed with a labyrinth seal. The effects of the gaps are discussed in the next paragraphs prior to the presentation of the drag data and the oil-flow photographs showing the gap effects.

The 0.246-inch (0.625-cm) gaps between the ends of the cylinder and the tunnel floor and ceiling were separated from the instrumented cylinder sections by fixed cylinder sections at least a diameter in length. Therefore, the effects of the end gaps on the measured forces are believed to have been insignificant. The 0.03-inch (0.762-mm) gaps between the fixed and instrumented cylinder sections caused extensive flow disturbances that affected the drag and lift data. The measurements taken on the smaller 0.1D instrumented section were totally unreliable. Also, there were large errors in the measurements taken on the 2.33D instrumented section. In an effort to eliminate these

disturbances, several methods of filling the gaps were tried. The sealing method used was to fill the gaps between the edges of the cylinder sections with a silicone rubber compound so as to present a flush surface to the airstream. The flexibility of this compound allowed relative movement between the instrumented and fixed cylinder sections. Although the shear load transmitted by the flexible rubber seal was only about 1 percent of the load on the 2.33D instrumented section, the load transmitted to the adjacent 0.1D section caused unacceptably large errors in the force measurements taken on the 0.1D section. Consequently, data from the 0.1D section are not presented. The original purpose of the 0.1D section was to compare the data from this cylinder section with the overall data from the large instrumented section to obtain some indication of any three-dimensional aspects of forces along the length of the cylinder and of the formation (if any) of vortex "cells" as discussed in reference 3.

The effects of the gaps on the flow are depicted in the oil-flow photographs of figure 7. For a mixed laminar and turbulent flow $\left(R_N \approx 2.5 \times 10^6\right)$, the separation is much more uniform with the gap-sealed flow. (Compare fig. 7(a) with fig. 7(b).) A similar comparison is made for turbulent flow conditions at $R_N \approx 10 \times 10^6$. (See fig. 7(c) and fig. 7(d).) Again, the gap-sealed separation is more uniform, but the gap-open flow was not as disturbed (fig. 7(c)) as in the mixed laminar and turbulent flow case (fig. 7(a)).

Table I presents mean drag coefficients measured on the 2.33D cylinder section with the gaps sealed and with the gaps open and also presents the section lift and drag coefficients obtained from integration of the static pressures in the lift and drag directions. Figure 8 presents selected drag data from table I. Gap-sealed and gap-open force data and integrated-static-pressure section-drag data are compared. At lower Reynolds numbers, the static-pressure data and force data, both taken with gaps open, are significantly higher than the force data with the gaps sealed. The oil-flow photograph in figure 7(a) suggests that even though the static orifices were 0.753 diameter below the unsealed gap, the flow in this area may have been affected by the gaps. Since figure 8 shows the drag-coefficient data obtained by force measurements on the cylinder with gaps open and those obtained by integration of the static pressures to be questionable, only gap-sealed drag data are presented in the rest of the report.

The speed of sound in freon is about one-half that in air, and the kinematic viscosity is about one-sixth that of air; consequently, the Mach number—Reynolds number relationship is different for the two test mediums at any given pressure. Therefore, when comparing drag data obtained in the two test mediums, air and freon, at various pressures, the following cross-plotting procedure was used to isolate Mach number and Reynolds number effects. For each series of data points taken with a given test medium and pressure, working plots of the type presented in figure 9 were constructed. One plot presents Reynolds number as a function of Mach number, and the other plot presents drag coefficient as a function of Mach number. Smooth curves were faired through the data points.

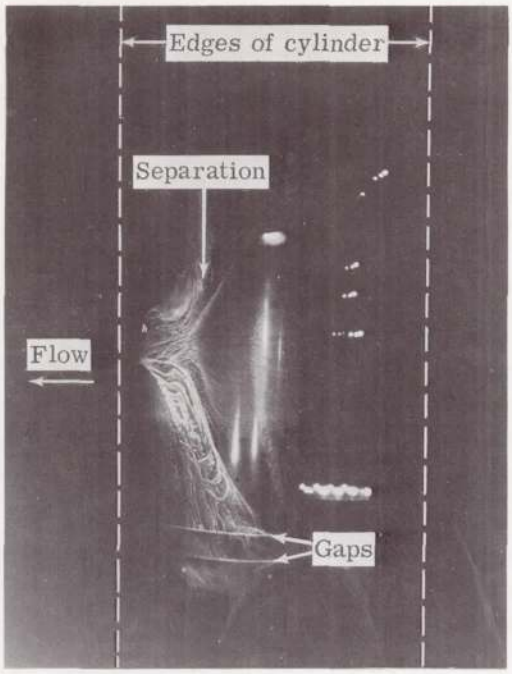

(a) Gaps open; $R_N = 2.3 \times 10^6$.

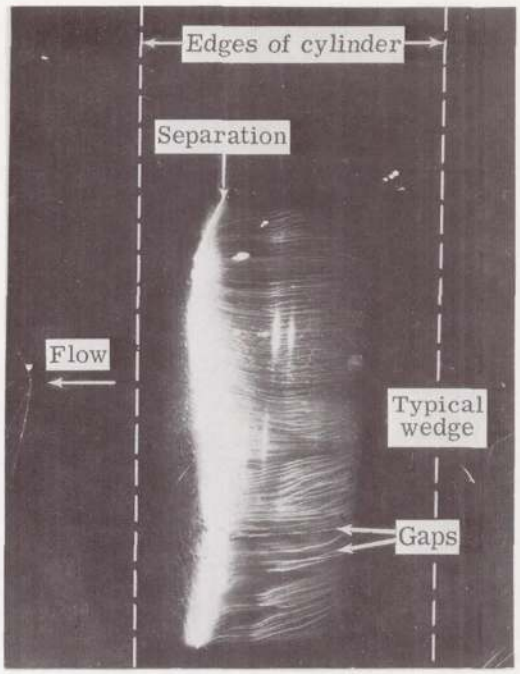

(b) Gaps sealed; $R_N = 2.9 \times 10^6$.

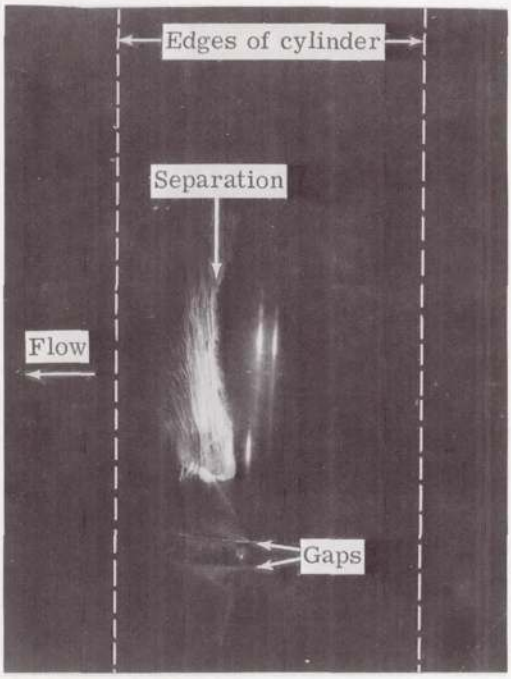

(c) Gaps open; $R_N = 10.2 \times 10^6$.

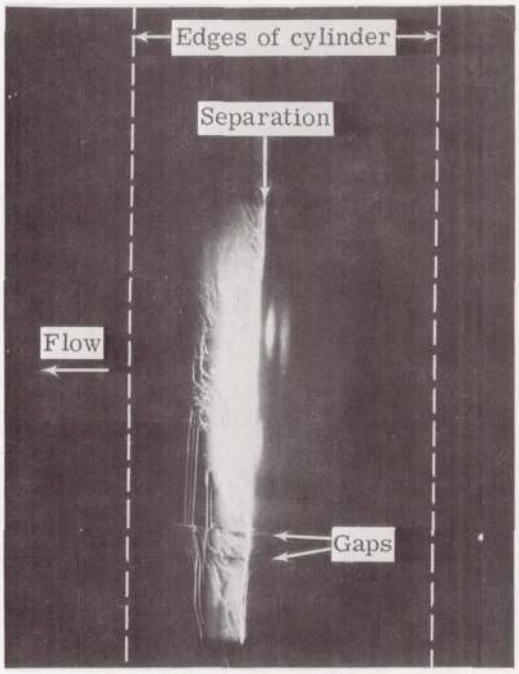

(d) Gaps sealed; $R_N = 9.5 \times 10^6$.

L-68-10,014

Figure 7.- Oil-flow photographs showing flow about cylinder at low and high Reynolds numbers for gaps-open and gaps-sealed conditions.

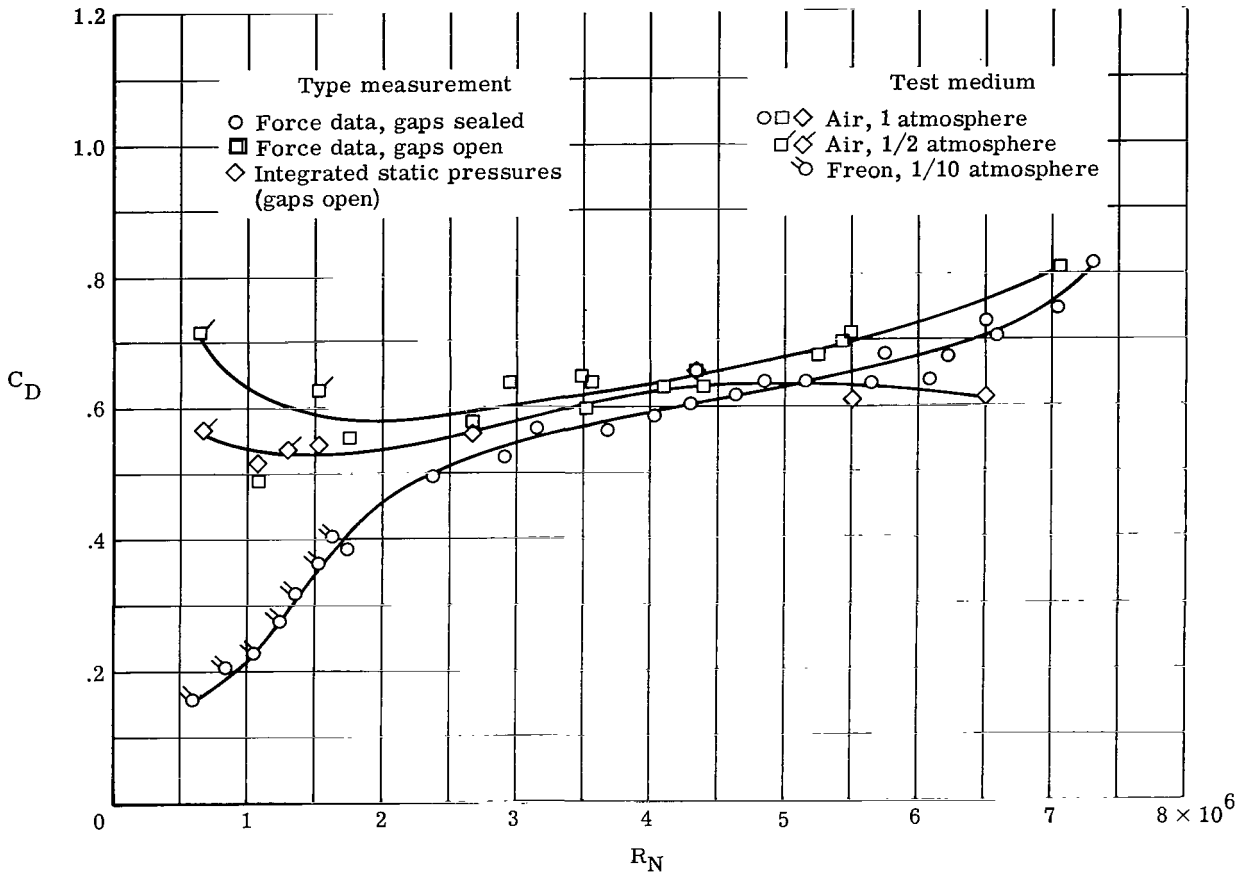

Figure 8.- Comparison of drag-coefficient data obtained by force measurements with gaps sealed, force measurements with gaps open, and by integration of static pressures.

Then, by using the faired curves at selected Mach numbers, the corresponding Reynolds numbers and drag coefficients were read. The results of this procedure are tabulated in table II.

Drag data from table II for $M \leq 0.2$ are presented in figure 10 and compared with data from previous investigations. These data are of particular interest for ground winds on launch vehicles or similar large cylindrical structures where Mach numbers are low but Reynolds numbers high. The trends from the four different sources agree well; however, at a given Reynolds number, the differences in measured drag coefficients are appreciable. In particular, the greater drag on Roshko's cylinder (ref. 5) as compared with the data of these tests was probably caused by the differences in roughness of the two cylinder surfaces. Roshko's cylinder had a sandblasted finish with a roughness height of 200 microinches (5.08 μm), which gave a roughness factor (roughness height to diameter) about 6 times that of the present cylinder. Schlichting (ref. 14) indicates that

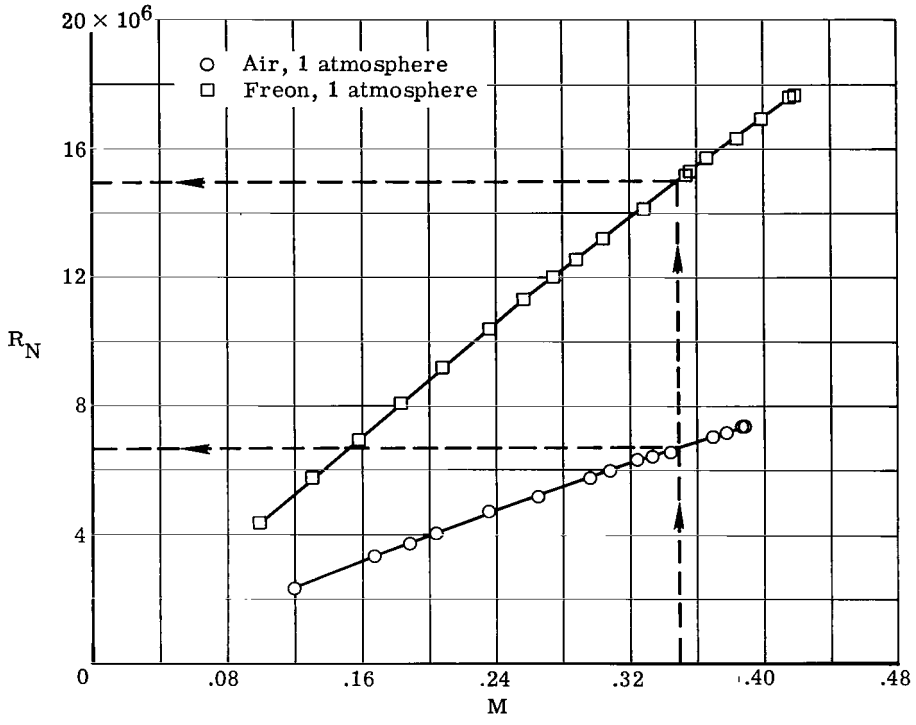

(a) Variation of Reynolds number with Mach number.

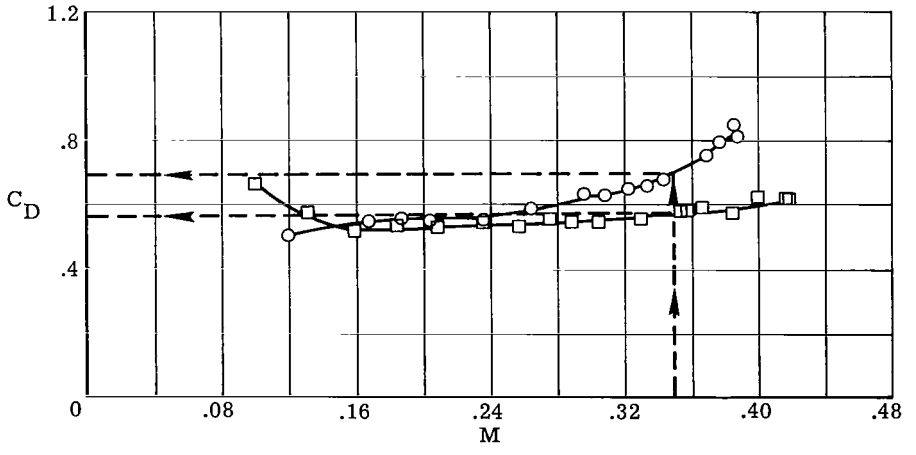

(b) Variation of drag coefficient with Mach number.

Figure 9.- Typical working plot of data from two tunnel runs in different test mediums.

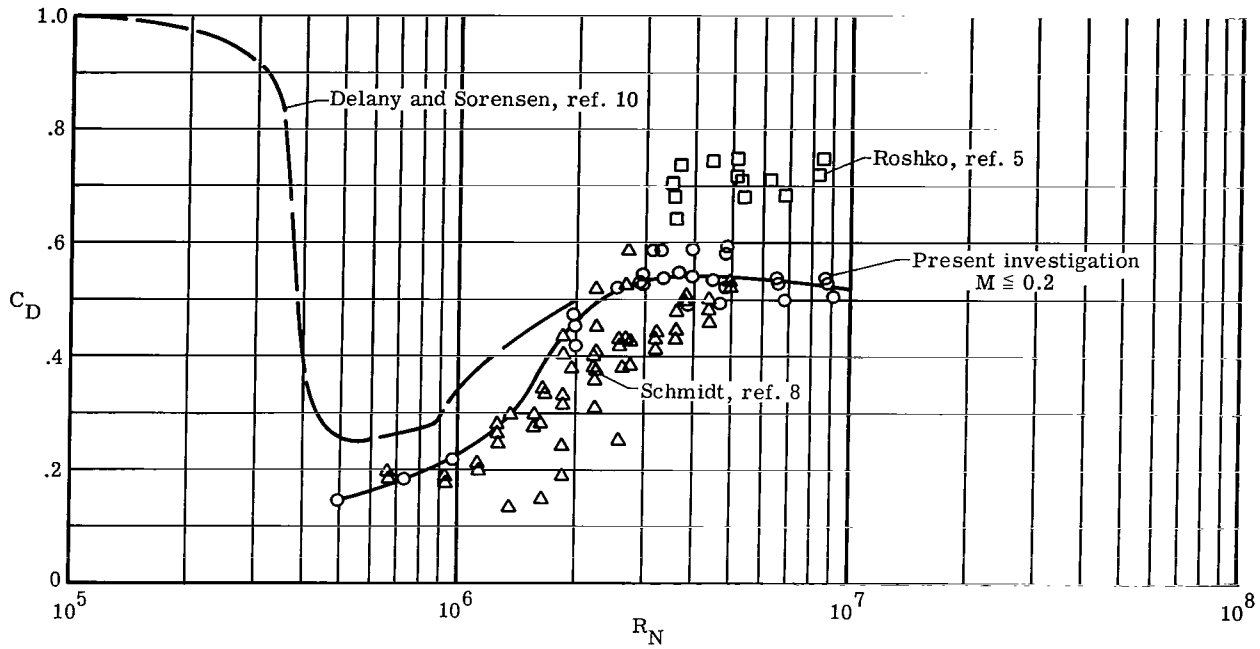

Figure 10.- Mean drag coefficient for $M \leq 0.2$ and comparison with previous investigations.

changes in drag of the order shown in figure 10 could be caused by this difference in roughness. The data of the present investigation show that for a smooth cylinder the drag coefficient increases from 0.15 at $R_N \approx 0.5 \times 10^6$ to about 0.54 at $R_N \approx 3 \times 10^6$ and then decreases slightly to 0.52 as Reynolds number increases to 10×10^6.

The variation of base pressure should have the same trend with Reynolds number as does the mean drag. The base-pressure-coefficient data at Mach number ≤ 0.2 are presented in figure 11, together with base-pressure data from references 5, 6, and 8. These base pressures show the same trends as the drag coefficients of figure 10, with the base-pressure data for the present investigation at Reynolds numbers greater than 2×10^6 in agreement with the data of Schmidt (ref. 8) but less negative than those of Roshko (ref. 5). The base pressures for the present investigation at $R_N \leq 2 \times 10^6$ may be affected by flow disturbances from gaps or surface imperfections as previously discussed.

The increase in drag coefficient between Reynolds numbers from 0.5×10^6 to 3×10^6 (fig. 10) occurs in the range of flow where, as Reynolds number increases, the turbulent transition moves upstream until it eliminates the laminar bubble and continues moving upstream. The turbulent boundary layer grows in thickness more rapidly than the replaced laminar boundary layer. This increased thickness results in a widened wake with a more negative base pressure (fig. 11) and a resultant increase in drag (fig. 10). As Reynolds number is increased above about 3×10^6, the thinning effect of Reynolds number

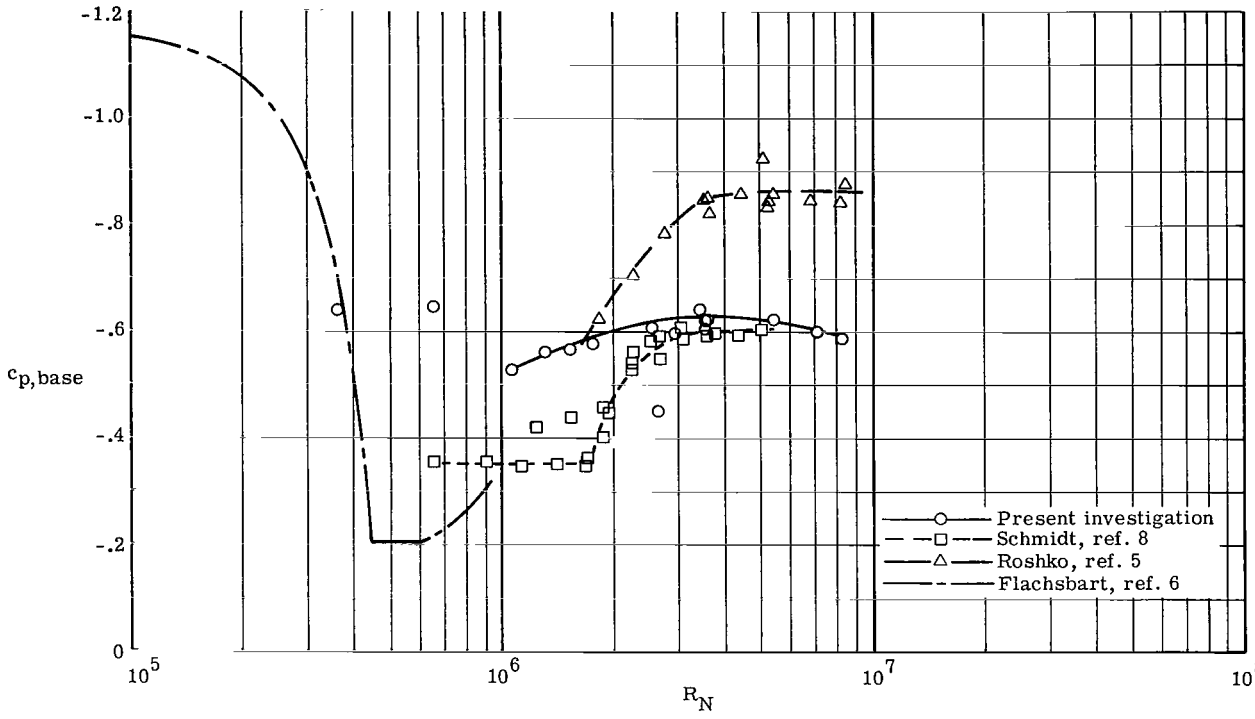

Figure 11.- Base-pressure-coefficient data at $M \leq 0.2$ and comparison with previous investigations.

on the boundary layer most likely exceeds the thickening effect of the small remaining upstream movement in transition as the transition nears the stagnation line. There is a resultant decrease in wake width, negative base pressure (fig. 11), and drag (fig. 10).

An interesting Mach number—Reynolds number effect on drag occurred as Mach number was increased from 0.2 to 0.4. As shown in figure 12 (which is plotted from the data of table II) at Reynolds numbers between 4×10^6 and 8×10^6, a peak in the variation of drag coefficient with Reynolds number develops at Mach numbers above 0.2. A plausible physical explanation of this peaking is suggested as follows. As the Mach number of the flow around the cylinder approaches the critical value (estimated from the local distribution of pressure to occur at a free-stream Mach number of 0.46), the compressibility effect on the distribution of pressure moves the flow separation forward with a resultant increase in negative base pressure and drag. Figure 13(a) indicates this drag rise due to Mach number at a Reynolds number of 7.5×10^6 as obtained from cross-plotting the data of figure 12. For a constant, free-stream Mach number, however, an increase in Reynolds number in the region around 7×10^6 will, as discussed in relation to figure 10, thin the boundary layer with a resultant rearward movement in separation, a narrowed wake, and a decrease in negative base pressure and drag. Figure 13(b) indicates this trend in drag at a Mach number of 0.4 as obtained from the data of figure 12. These

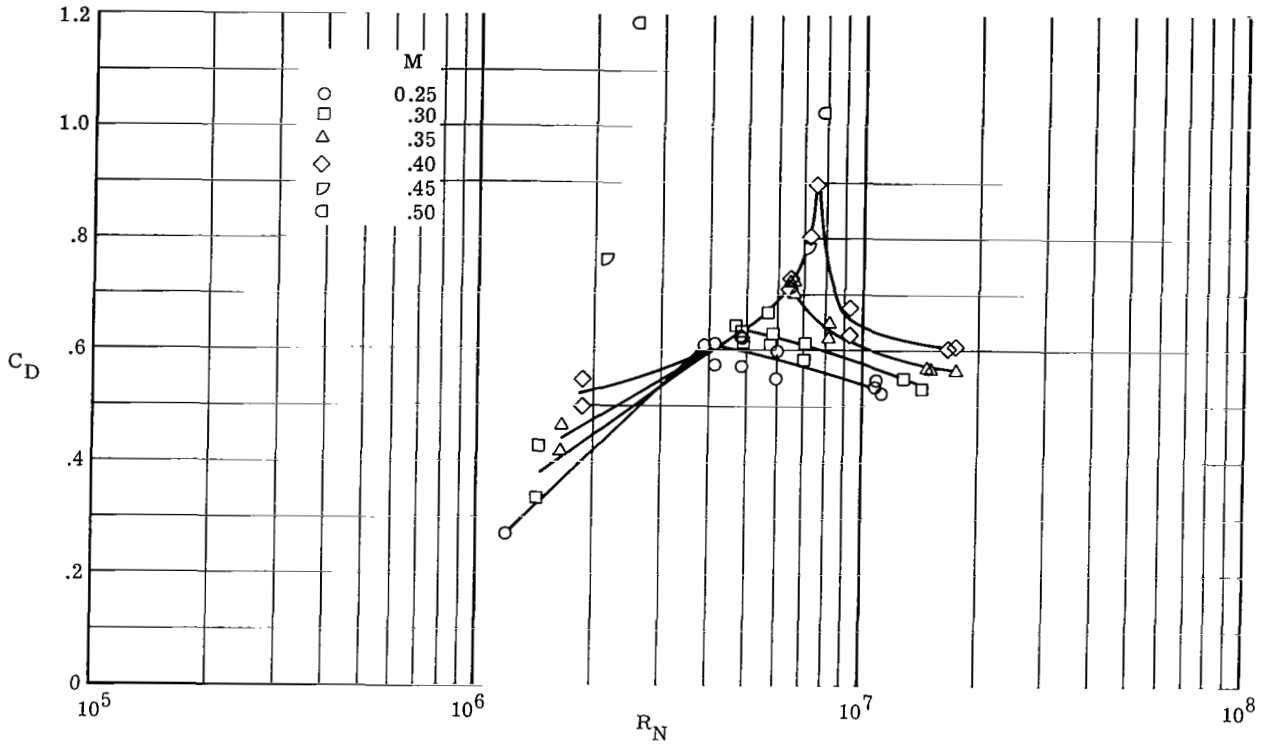

Figure 12.- Variation of drag coefficient with Reynolds number for several constant Mach numbers between 0.25 and 0.50 (from table II).

counteracting effects of M and R_N probably result in the peaks shown in figure 12. It is also of interest to note that for free-stream Mach numbers equal to or greater than critical, the adverse compressibility effect on flow separation is considerably greater than the favorable effect of Reynolds number, as indicated by the large drag increases shown by the isolated test points in figure 12 for Mach numbers of 0.45 and 0.50.

The effects of cylinder lateral oscillation on the mean drag coefficients are shown in figure 14. For this set of data, the cylinder was first held stationary and drag measurements taken; then the cylinder was forced by the hydraulic shakers at either end to oscillate perpendicularly to the airflow with an amplitude of 0.5 inch (1.27 cm) at 10 hertz corresponding to $\frac{h_0}{D} = 0.014$. The test medium was atmospheric air. Examination of figure 14 shows that within the range of data presented, cylinder motion in the lift direction had no significant effect on the mean drag. The drag data were measured at other cylinder amplitudes and frequencies, but again the motion had no significant effect on the mean drag.

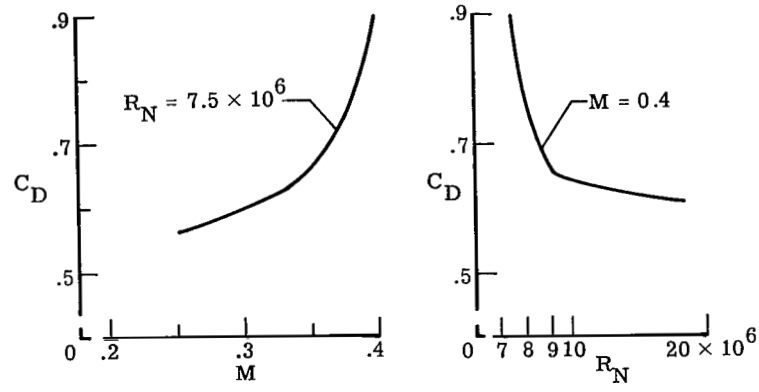

(a) Drag increase due to Mach number.

(b) Drag decrease due to Reynolds number.

Figure 13.- Peak in drag coefficient expressed as combined effect of Mach number and Reynolds number.

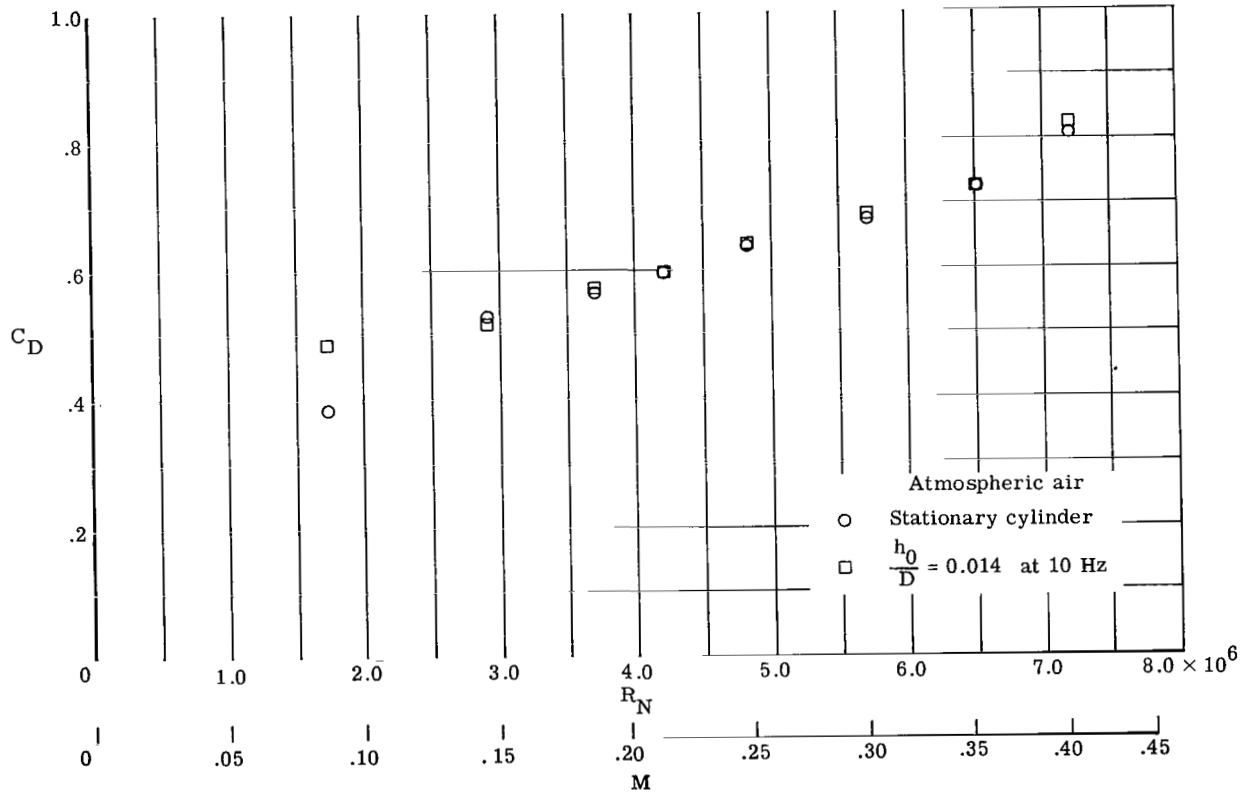

Figure 14.- Effects of cylinder lateral oscillation on mean drag coefficient.

Characteristics of Unsteady Lift Measured on Stationary Cylinder

The results discussed thus far have been for static-pressure distributions and mean drag forces that were handled in a conventional manner. In the rest of the paper, the results presented are for the unsteady lift forces.

The time history of unsteady lift acting on a stationary cylinder in a flow may be completely random, periodic, or some mixture of random and periodic. In order to select appropriate characteristics to describe the unsteady lift in this presentation, it was first necessary to determine the nature of the unsteady-lift time history. A system of classifying or categorizing the unsteady lift was devised and was based on examination of several different characteristics of the variation of lift with time. In the subsequent section, this classification system is discussed in connection with a description of the frequency content of the unsteady lift. Then the magnitude of the unsteady lift on the stationary cylinder is described.

Frequency content of unsteady lift.- In this paper, the frequency content of the unsteady lift force is described in two ways. The more conventional way of expressing the frequency content is in terms of the nondimensional aerodynamic Strouhal number $S = \frac{f_S D}{V}$, where f_S is the vortex-shedding frequency of the cylinder. This frequency is determined from the frequency of the autocorrelation function of the time-history data samples of the unsteady lift force. The other method of describing the frequency content of the unsteady lift force is in terms of a Strouhal bandwidth. If the vortex-shedding frequency is defined to be the frequency of the main peak in a power-spectral-density plot obtained from a data sample of the unsteady lift force, the frequency interval between the half-power points of this spectrum peak is defined as the Strouhal bandwidth. Another indication of the periodicity of unsteady lift force was given by studying plots of the amplitude probability density distribution of the unsteady-lift-force data samples. Examination of the time histories, power spectral densities, autocorrelation functions, and probability density functions of the data samples of the unsteady lift force led to the conclusion that the unsteady lift forces on the cylinder could be grouped into three regimes. These regimes are termed wide-band random, narrow-band random, and quasi-periodic. The classification of the unsteady lift force into these regimes may be determined from the autocorrelation function according to the following criteria:

(1) Wide-band random – Autocorrelation function has no more than one peak, other than the $\tau = 0$ peak.

(2) Narrow-band random – Autocorrelation function has two or more consecutive peaks, and the percentage decrement between peaks is greater than 10 percent.

(3) Quasi-periodic – Over the range of time lags analyzed, the decrement in consecutive peaks in the autocorrelation function is less than 10 percent.

A typical data sample from each of these regimes is presented in figure 15 in the form of the time history, the power spectral density, the autocorrelation function, and the amplitude probability density distribution.

The correspondence between the various regimes and Reynolds number is as follows: At the lower Reynolds numbers between approximately 1.1×10^6 and 3.5×10^6, the unsteady lift forces are predominantly wide-band random. In terms of previous investigations (for example, refs. 2, 5, and 8), the wide-band forces occur in the "supercritical" Reynolds number range. At Reynolds number above approximately 6×10^6, the unsteady lift forces are quasi-periodic. At intermediate Reynolds numbers, that is, between approximately 3.5×10^6 and 6×10^6, the term narrow-band random is used to denote the intermediate regime between wide-band random and quasi-periodic. The quasi-periodic lift forces occur in the "transcritical" Reynolds number range of reference 5.

In order to illustrate the variations of Strouhal bandwidth with Reynolds number, figure 16 presents the half-power Strouhal bandwidth of the unsteady lift for three ranges of Mach number. For Mach numbers up to about 0.4, the Strouhal bandwidth variation with Reynolds numbers is as follows: At Reynolds numbers up to about 3.5×10^6, the Strouhal bandwidth is large; as Reynolds number increases from 3.5×10^6 to about 6×10^6, the Strouhal bandwidth narrows rapidly; and, at Reynolds numbers above 6×10^6, the Strouhal bandwidth is small. Also shown in figure 16 is a large Mach number effect on the Strouhal bandwidth at Reynolds numbers of about 2×10^6. A large, very rapid decrease occurs in bandwidth as Mach number is increased from 0.399 to 0.416. (See labeled test points.) Also, at Reynolds numbers above about 6×10^6, a slight decrease in bandwidth is noted as Mach number is increased.

Previous investigators have presented frequency characteristics in terms of a single Strouhal number rather than a Strouhal bandwidth. For purposes of comparison, the data are presented in terms of the variation of aerodynamic Strouhal number with Reynolds number. Since the Strouhal number is affected by both Mach number and Reynolds number and the values were obtained from tests in different densities and test mediums, the data were cross-plotted in the same manner as the steady drag (fig. 9) in order to separate Reynolds number and Mach number effects. Figure 17 and table III give the resultant cross-plotted data of Strouhal number as a function of Reynolds number at selected Mach numbers. Also presented in figure 17 are Strouhal number data obtained by other investigators (refs. 5, 9, and 10) at $M < 0.3$. The data of the present investigation agree with other investigations and in particular with those of Roshko (ref. 5) in the Reynolds number range from 3.7×10^6 to 8.4×10^6. This agreement occurs within the regions where a definite vortex-shedding frequency could be detected, as indicated by the shaded areas. At hitherto unexplored Reynolds numbers from 8×10^6 to 17×10^6, the Strouhal number is approximately constant at a value of about 0.3. In the Reynolds number range from about 0.5×10^6 to 3×10^6, the data exhibited no distinct frequency and all the investigators

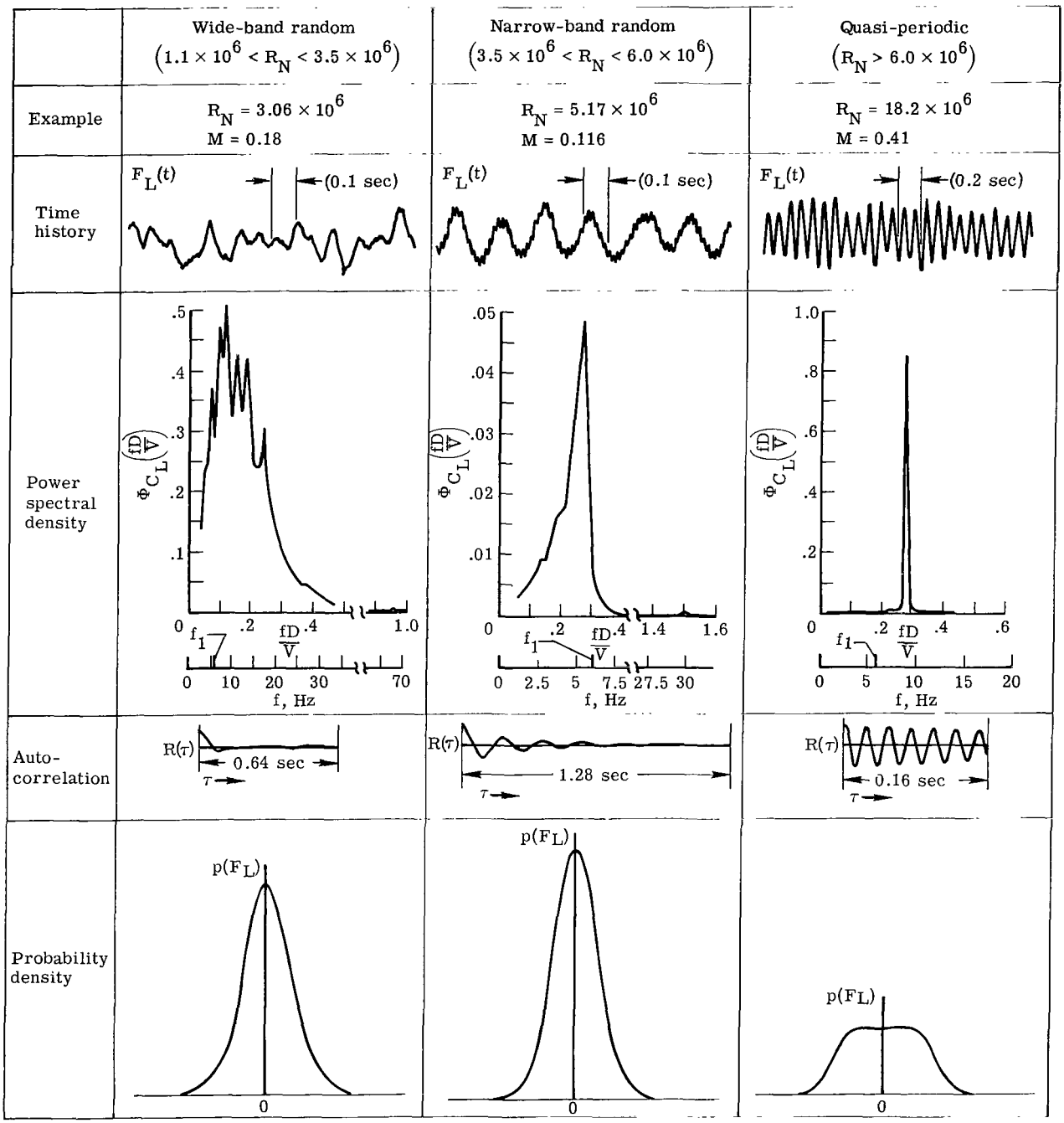

Figure 15.- Characteristic functions of unsteady lift force on stationary cylinder as presented for each classification regime.

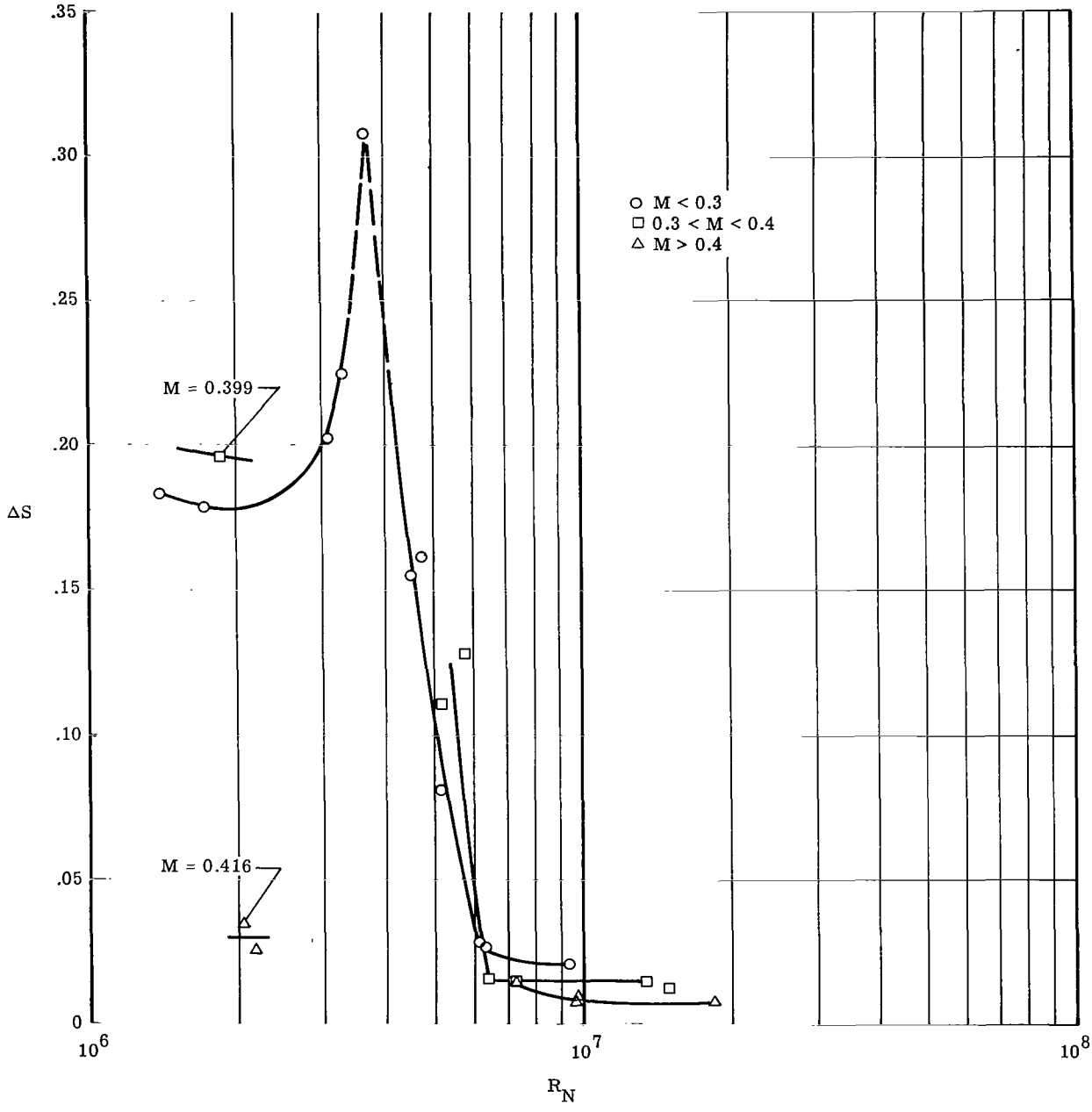

Figure 16.- Variation, for three ranges of Mach numbers, of Strouhal bandwidth of unsteady lift on stationary cylinder with Reynolds number.

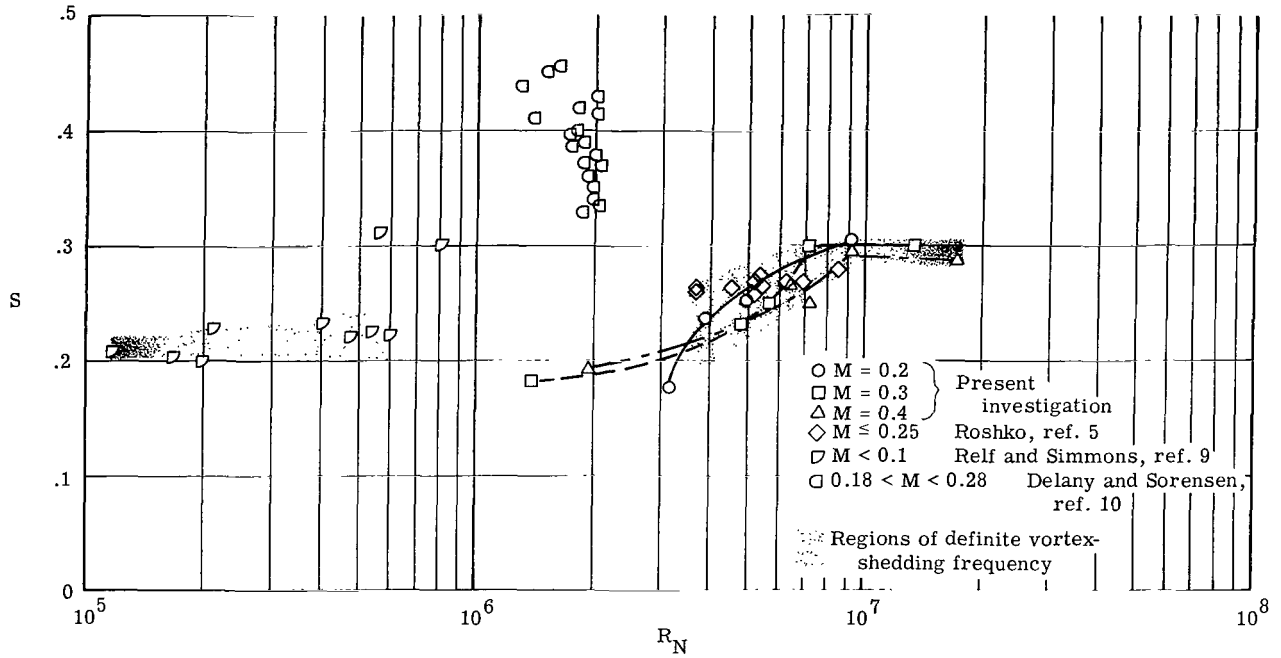

Figure 17.- Variation of Strouhal number of unsteady lift force on stationary cylinder with Reynolds number and comparison with previous investigations.

had difficulty in obtaining an identifiable dominant frequency. Accordingly, the agreement between the data in this Reynolds number range is poor. Schmidt (ref. 8) and Fung (ref. 2) measured unsteady lift forces at Reynolds numbers within this range, and they detected no predominant frequencies even though Schmidt's data are at Reynolds numbers up to 5×10^6.

This periodicity, or lack of it, is shown in another form in figure 18, which presents a comparison of power spectral densities of the lift force of the present investigation at Reynolds numbers of about 1×10^6 and 5×10^6 with power spectral densities of similar Reynolds numbers from the data of Schmidt (ref. 8) and Fung (ref. 2). As just discussed, none of the investigators show periodicity in the form of distinct energy peaks at Reynolds number of about 1×10^6. At Reynolds number of about 5×10^6, the results of the present investigation show a definite energy peak but those of Schmidt (ref. 8) do not. Such apparent discrepancies are probably to be expected in this narrow-band random regime, which is a transition between the wide-band random and quasi-periodic regimes. In the narrow-band random regime, boundary-layer transition is still a variable with Reynolds number. Therefore, the unsteady lift may be highly sensitive to small differences in flow conditions such as surface irregularities and tunnel turbulence levels.

Magnitude of unsteady lift.- The root-mean-square values of lift coefficient were computed from the value of the autocorrelation of the lift force at zero time lag ($\tau = 0$).

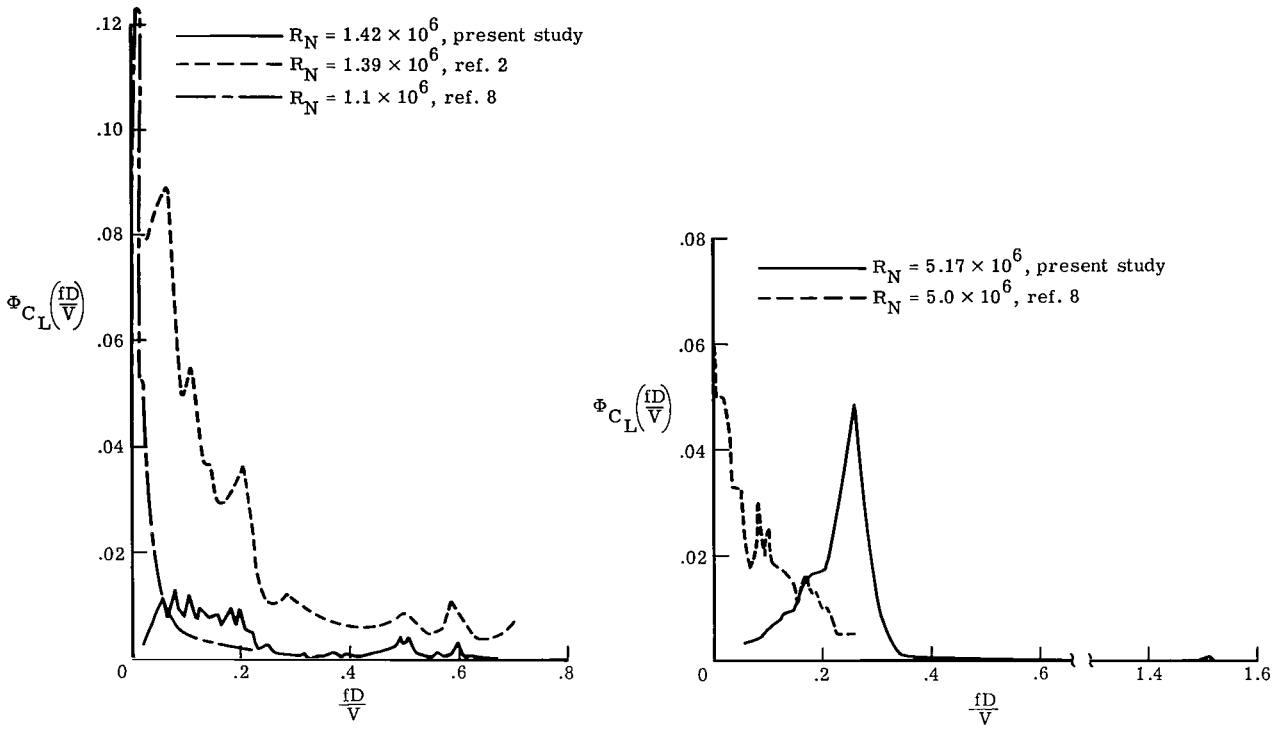

(a) Power spectral densities at $R_N \approx 1.3 \times 10^6$.

(b) Power spectral densities at $R_N \approx 5 \times 10^6$.

Figure 18.- Power spectral density of unsteady lift force measured on stationary cylinder at Reynolds numbers of 1.42×10^6 and 5.17×10^6, and comparison with previous investigations.

These autocorrelation values were checked by a time-averaged, mean-square analyzer. Both Mach number and Reynolds number affect the unsteady lift coefficients as was the case for the mean drag and Strouhal number data. Therefore, the same type of cross-plot scheme as used for drag and Strouhal number was used on the unsteady-lift-coefficient data to separate the Mach number and Reynolds number effects. Table IV presents the values of $C_{L,rms(0)}$ from which the cross plots were made. Figure 19 presents the data determined from the working plots. In this figure, the stationary-cylinder root-mean-square lift coefficients at $M \leq 0.3$ and $M = 0.4$ are presented as functions of Reynolds number. Examination of this figure shows that for the data at $M \leq 0.3$, the unsteady lift appears to be multiple-valued at Reynolds numbers between about 1.4×10^6 and 8×10^6. This trend toward scatter in these regions of Reynolds number was true for all test mediums and densities for which data were recorded at Mach numbers less than 0.3. Delany and Sorensen (ref. 10) show a similar scatter in drag data which is attributed to changes from a symmetric to an asymmetric flow around the cylinder (see ref. 5).

As previously discussed, the static-pressure-distribution data indicated the existence at lower Reynolds numbers of substantial positive or negative steady lift coefficient

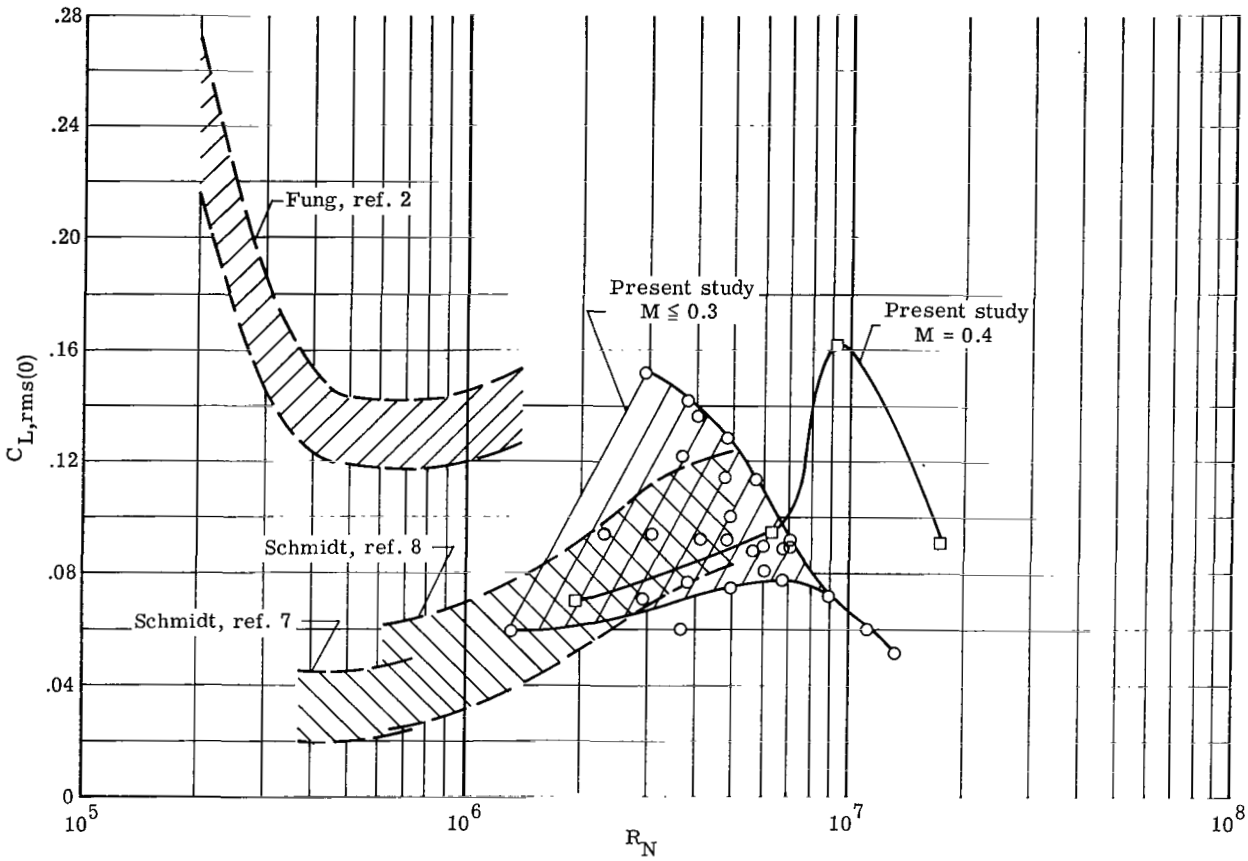

Figure 19.- Stationary-cylinder root-mean-square lift coefficient at $M \leqq 0.3$ and $M = 0.4$ presented as a function of Reynolds number and compared with previous investigations.

values. These phenomena were explained in terms of a possible asymmetry in the laminar flow caused by asymmetric disturbances, such as turbulence wedges occurring on the cylinder. This same mechanism is thought to be responsible for the double values of root-mean-square unsteady lift coefficient. Such conjecture cannot be proven on the basis of present evidence, since oil-flow photographs show only one side of the model. However, it appears to be a reasonable assumption that, in the region of scatter or multiple-valued data, the various values of root-mean-square lift coefficients are associated with variations of symmetry of the flow. Note in figure 19 that the two boundaries merge at about a Reynolds number of 8×10^6, and the merged boundary gradually decreases in value as Reynolds number is increased. Thus, the multiple data seem to occur at Reynolds numbers corresponding to those for the wide-band and narrow-band regimes and merge to a single-valued boundary in the quasi-periodic regimes of Reynolds number.

At a Mach number of 0.4, the root-mean-square lift coefficient has less scatter, and there is a large Mach number effect at Reynolds numbers from 7×10^6 to 17×10^6 as

shown by a rounded peak in the data at a Reynolds number of about 9×10^6. This peak corresponds roughly to the similar peaks in drag data at this Mach number, and may be associated with the same counteracting effects of Mach number and Reynolds number on boundary-layer separation discussed previously.

Also presented for comparison in figure 19 are the unsteady-lift-coefficient values from references 2, 7, and 8. These data are presented in the form of broad bands because of scatter in the individual data points. Both sets of comparative data tend to merge into the data of the present investigation. Fung's data (ref. 2) approach the upper part of the multiple-valued region and Schmidt's data (refs. 7 and 8) merge with the lower part of this region. Thus, the unsteady lift coefficients obtained on the stationary cylinder are consistent with the trends of previous data.

Measurement of Unsteady Lift Due to Cylinder Motion

As previously described, a positive displacement sinusoidal oscillation in the lift direction was imparted to the model by the hydraulic shakers at the top and bottom of the cylinder. The model was driven at frequencies from 3 to 18.7 hertz and amplitudes up to 3 inches (7.62 cm). The forces in the lift direction were measured on the 2.33D-length instrumented section by using the ICB system, and the data thus obtained were reduced by using techniques described in appendix B.

The unsteady lift forces on the moving cylinder are described in terms of some of the same characteristics used to describe the unsteady lift on the stationary cylinder. A comparison of the power spectral densities of the lift force on the cylinder with and without motion is presented first. Next, under an assumption that the unsteady lift due to motion had a sinusoidal component related to the motion of the cylinder, an analysis is made which determines the in-phase and 90° out-of-phase (real and imaginary) components of the unsteady-lift-force vector with respect to displacement at the frequency of motion. Finally, these components are interpreted in terms of aerodynamic derivatives. The basic reduced data from which these analyses are presented are given in table V.

Power spectral density and root-mean-square values.- Figure 20 presents the power spectral density of the aerodynamic lift coefficient for two data points at the same Mach number and Reynolds number. For one data sample, the cylinder was held stationary; whereas, for the other data sample, the cylinder was oscillated at the aerodynamic Strouhal number (S = 0.31) for the stationary cylinder. A large increase in the peak of the spectrum for the oscillating cylinder at $\frac{fD}{V} = 0.31$ is readily apparent. The root-mean-square lift coefficient increased from 0.076 to 0.130. Thus, this comparison shows the existence of a lift due to motion. Of interest in figure 20(b) is the small hump at $\frac{fD}{V} = 0.6$, which indicates a small second harmonic content.

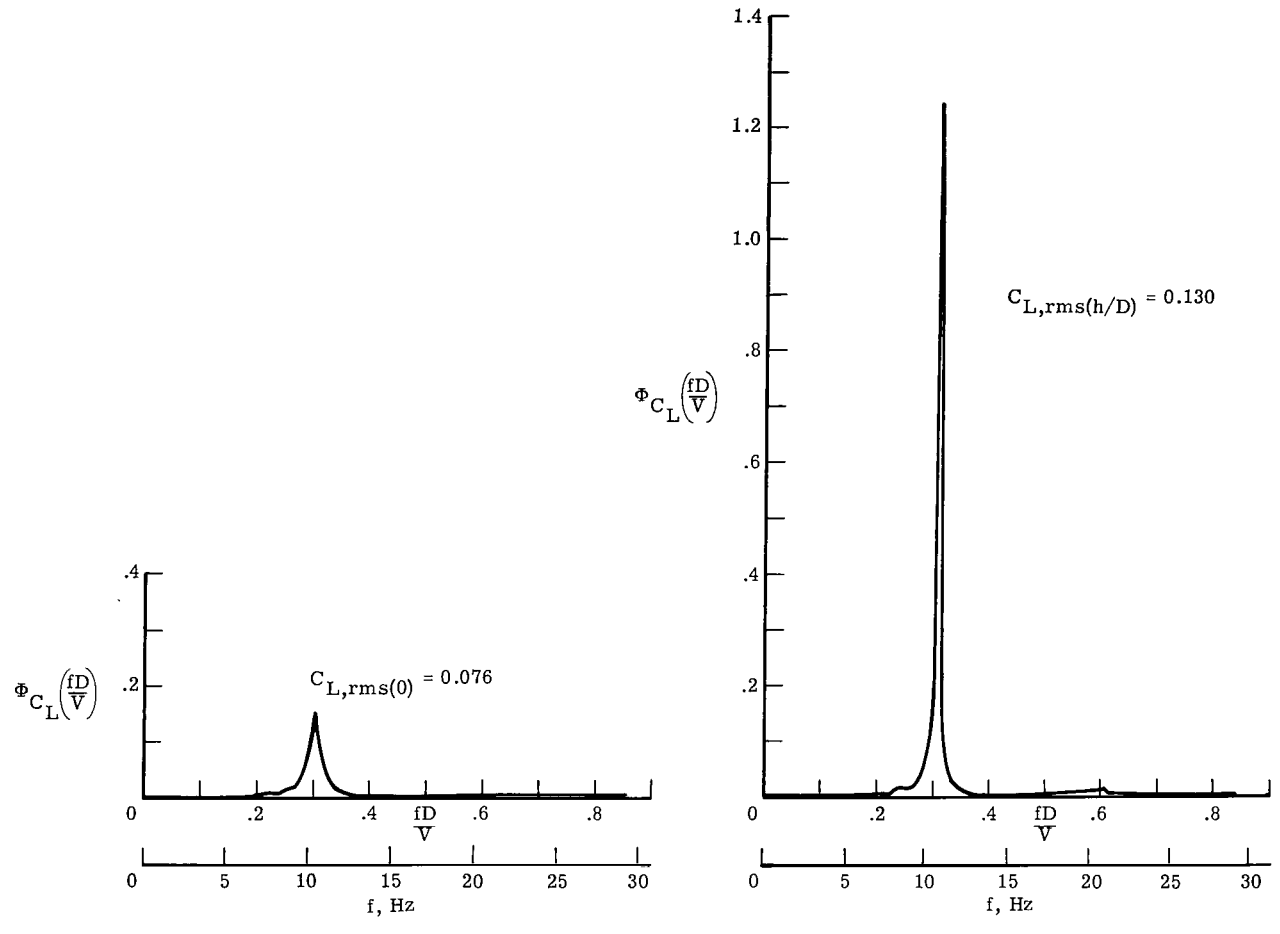

(a) No cylinder motion; $R_N = 9.33 \times 10^6$; $M = 0.20$.

(b) Cylinder oscillation at $\frac{h_0}{D} = 0.0278$; $f_h = 10.5$ hertz; $R_N = 9.33 \times 10^6$; $M = 0.20$.

Figure 20.- Effect of cylinder lateral oscillation on unsteady lift as shown by power spectral densities of unsteady lift measured with and without cylinder motion at same flow conditions.

In order to determine the magnitude of the unsteady lift due to oscillation of the cylinder, the ratio of the unsteady lift for the oscillating cylinder to the unsteady lift for the stationary cylinder was evaluated. This ratio was determined by taking selected values of the root-mean-square lift coefficient for the oscillating cylinder and normalizing them by the root-mean-square lift coefficient for the stationary cylinder at the same flow conditions. The results are plotted in figure 21 as functions of a nondimensional frequency ratio and amplitude of motion. The frequency ratio is the nondimensional forcing frequency of cylinder oscillation divided by the Strouhal number for the stationary cylinder $\left(\frac{f_h D}{V}\Big/S\right)$. The data selected for figure 21 and for subsequent figures have been restricted to Mach numbers less than 0.3 and Reynolds numbers above 5.5×10^6 where Mach number effects are small and the periodicity of the flow is clearly defined.

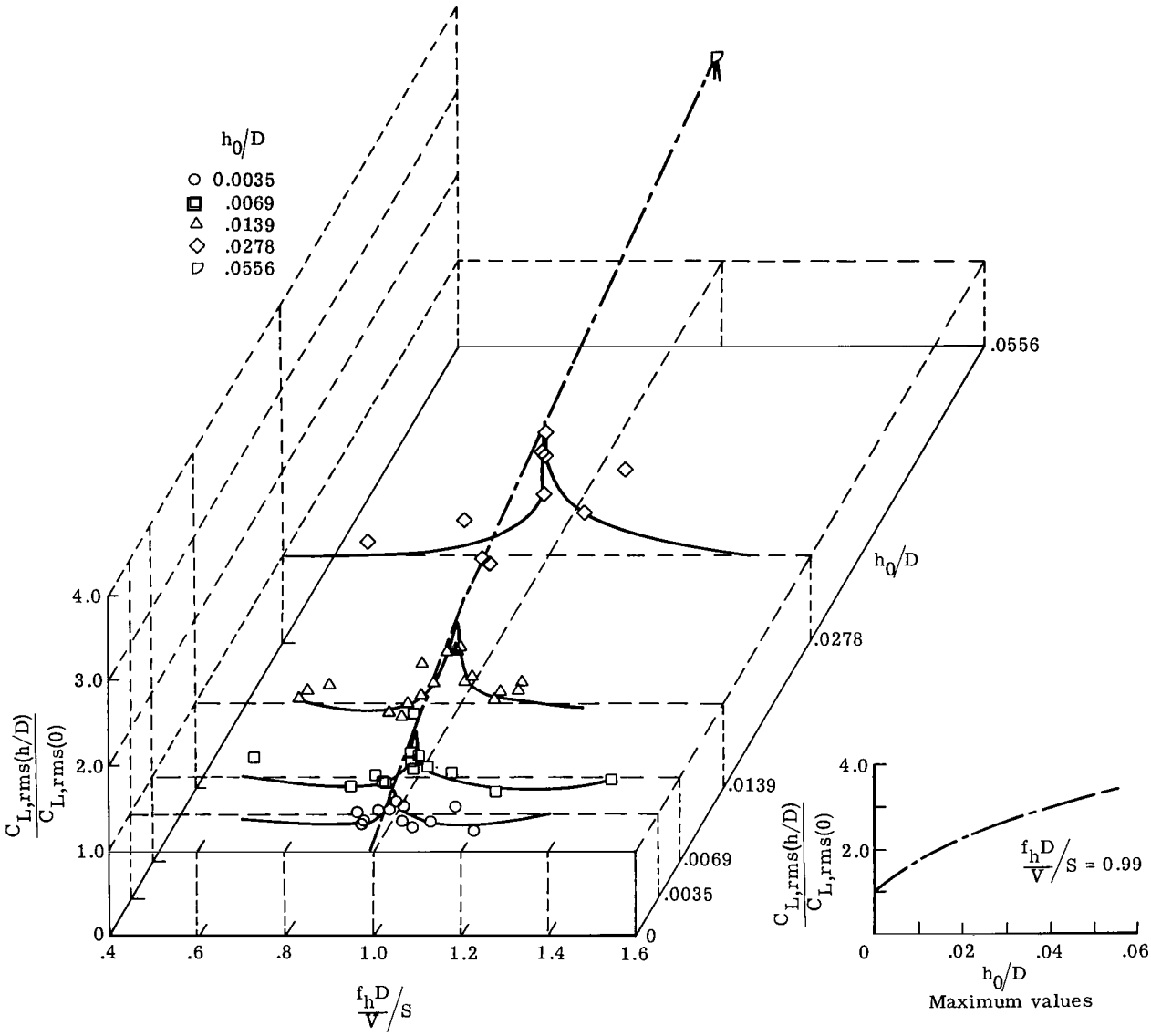

Figure 21.- Effects of forced cylinder oscillation on wide-band root-mean-square lift coefficient for oscillating cylinder normalized by lift coefficient for stationary cylinder.

The lift-coefficient ratios presented in figure 21 show that when the cylinder is oscillated in the lift plane at frequencies far removed from the aerodynamic Strouhal frequency there is no increase, or in some cases a slight decrease, in lift coefficient over that of the fixed cylinder. However, for cylinder motion at or near the Strouhal frequency there is a definite lift due to motion and this lift increases with amplitude of cylinder motion. The maximum amplification of the lift due to motion occurs when the frequency ratio is approximately equal to 0.99 and varies with h_0/D as indicated by the plot at the

lower right-hand side of figure 21. As shown by this variation of lift-coefficient ratio, the lift on the oscillating cylinder may increase to values several times the lift on the stationary cylinder.

Lift-force vector at frequency of cylinder oscillation.- Examination of data such as those given in figures 20 and 21 and of the time histories of the lift force on the oscillating cylinder indicates the likelihood of substantial correlation between the aerodynamic forces and cylinder motion. Therefore, an analysis was made which determined the aerodynamic force components that are in phase (real component) and 90^{o} out of phase (imaginary component) with the oscillatory displacement. These data are presented in figure 22(a) as the vector amplitude of the motion-dependent lift coefficient $\left(\left|C_L\right| = \left|C_{L,Re} + iC_{L,Im}\right|\right)$ and in figure 22(b) as the phase angle $\left(\theta = \tan^{-1}\frac{C_{L,Im}}{C_{L,Re}}\right)$ between the lift-coefficient vector and the cylinder displacement. An alternate representation of the same data is presented in figure 23 in terms of the real and imaginary vector components. Figures 22 and 23 also show that the unsteady-lift-due-to-motion vector is substantial only when the cylinder oscillates at or near the aerodynamic Strouhal frequency. This lift increases with increasing amplitude (fig. 22(a)). The phase angle of this lift-force vector (fig. 22(b)) has a large rapid shift as the cylinder frequency approaches and passes through the stationary-cylinder Strouhal frequency. This large phase shift indicates a basic change in the lift force from an unstable to a stable character. Examination of figure 23(a) indicates that the real component behaves much as the magnitude of the lift-coefficient vector does. (See fig. 22(a).) This force component, being in phase with displacement, may be thought of as an aerodynamic stiffness parameter. Similarly, the imaginary component (fig. 23(b)), being in phase with the cylinder velocity, may be regarded as an aerodynamic damping parameter. When the cylinder is oscillated at frequencies below the Strouhal frequency, the aerodynamic damping is destabilizing. As the cylinder frequency passes through the Strouhal frequency, there is an abrupt change to a stabilizing aerodynamic damping force.

Aerodynamic derivatives of lift due to motion.- The real and imaginary components of the lift-force vector were converted to aerodynamic derivatives h_a and k_a as used by Scruton in reference 4. The basic equation is

$$\text{Lift per unit length} = -2S^2qh\left(h_a + i2\pi k_a\right)$$

and the relationships between Scruton's derivatives and the real and imaginary components of the aerodynamic-lift-coefficients of figure 23 are

$$-h_a = \frac{C_{L,Re}}{2S^2(h/D)} \quad ; \quad -k_a = \frac{C_{L,Im}}{4\pi S^2(h/D)}$$

These derivatives are presented in figure 24 as functions of nondimensional frequency ratio and amplitude. Both $-h_a$ (fig. 24(a) and $-k_a$ (fig. 24(b)) are seen to vary

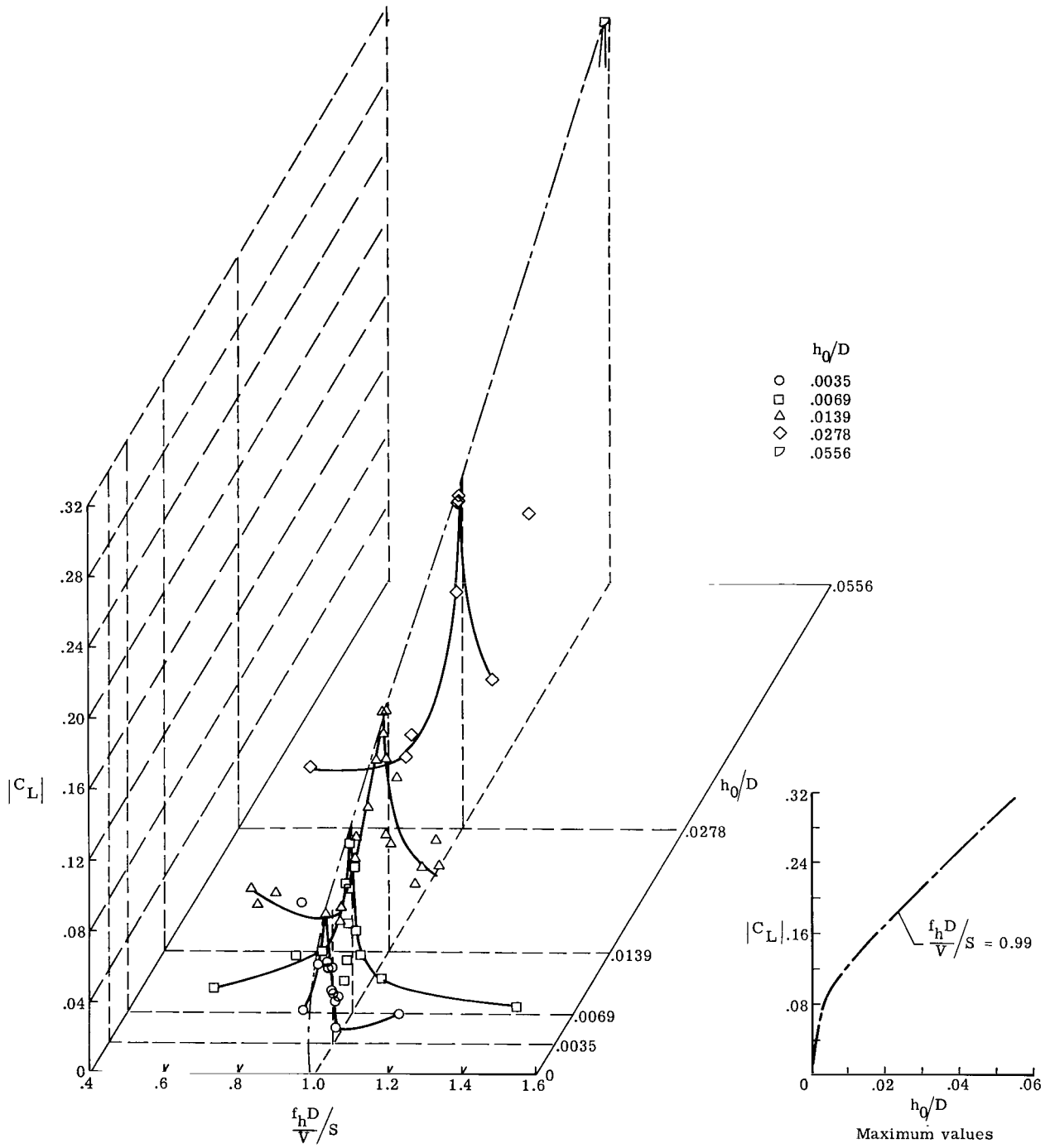

(a) Magnitude of lift-coefficient vector $|C_L|$ as a function of $\frac{f_h D}{V}/S$ and h_0/D.

Figure 22.- Variation of aerodynamic-lift-coefficient vector with the frequency of the cylinder oscillation.

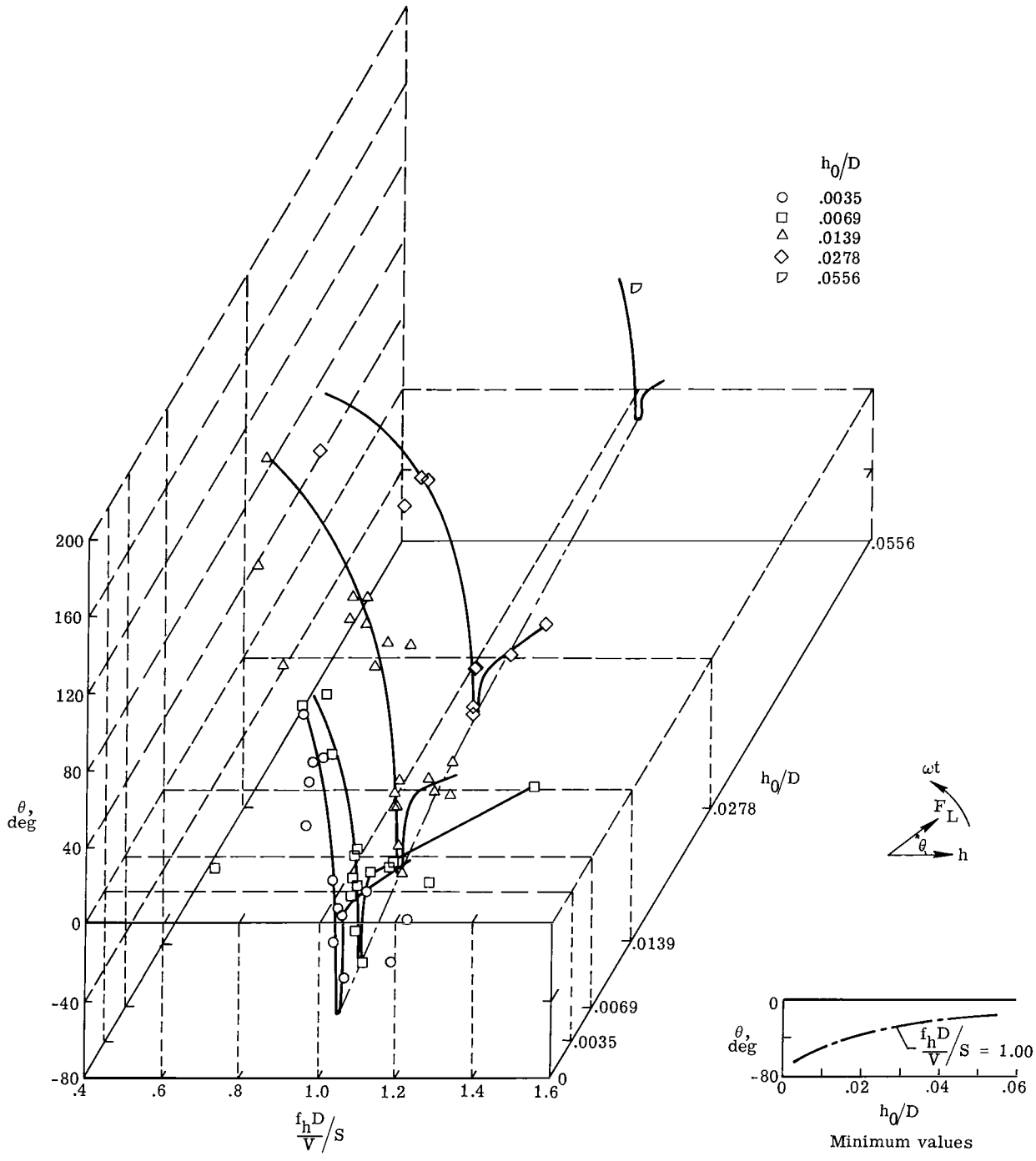

(b) Variation of phase angle between lift force and displacement with $\frac{f_h D}{V}/S$ and h_0/D.

Figure 22.- Concluded.

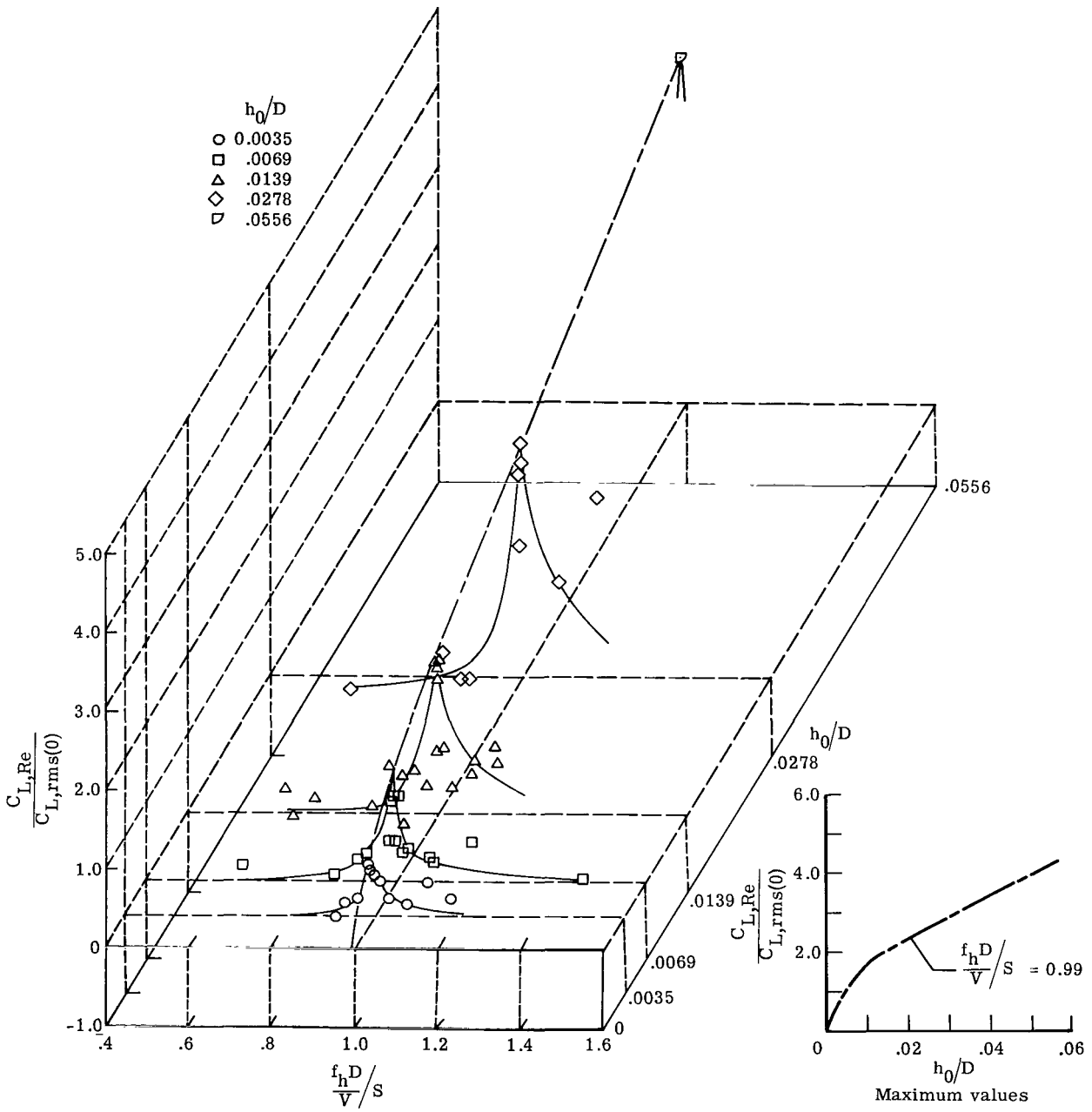

(a) Variation of $\frac{C_{L,Re}}{C_{L,rms(0)}}$ with $\frac{f_h D}{V}/S$ and h_0/D.

Figure 23.- Real and imaginary components of lift coefficient at cylinder forcing frequency normalized by wide-band root-mean-square lift coefficient on stationary cylinder.

Note: Lift per unit length = $(C_{L,Re} + iC_{L,Im})qD$.

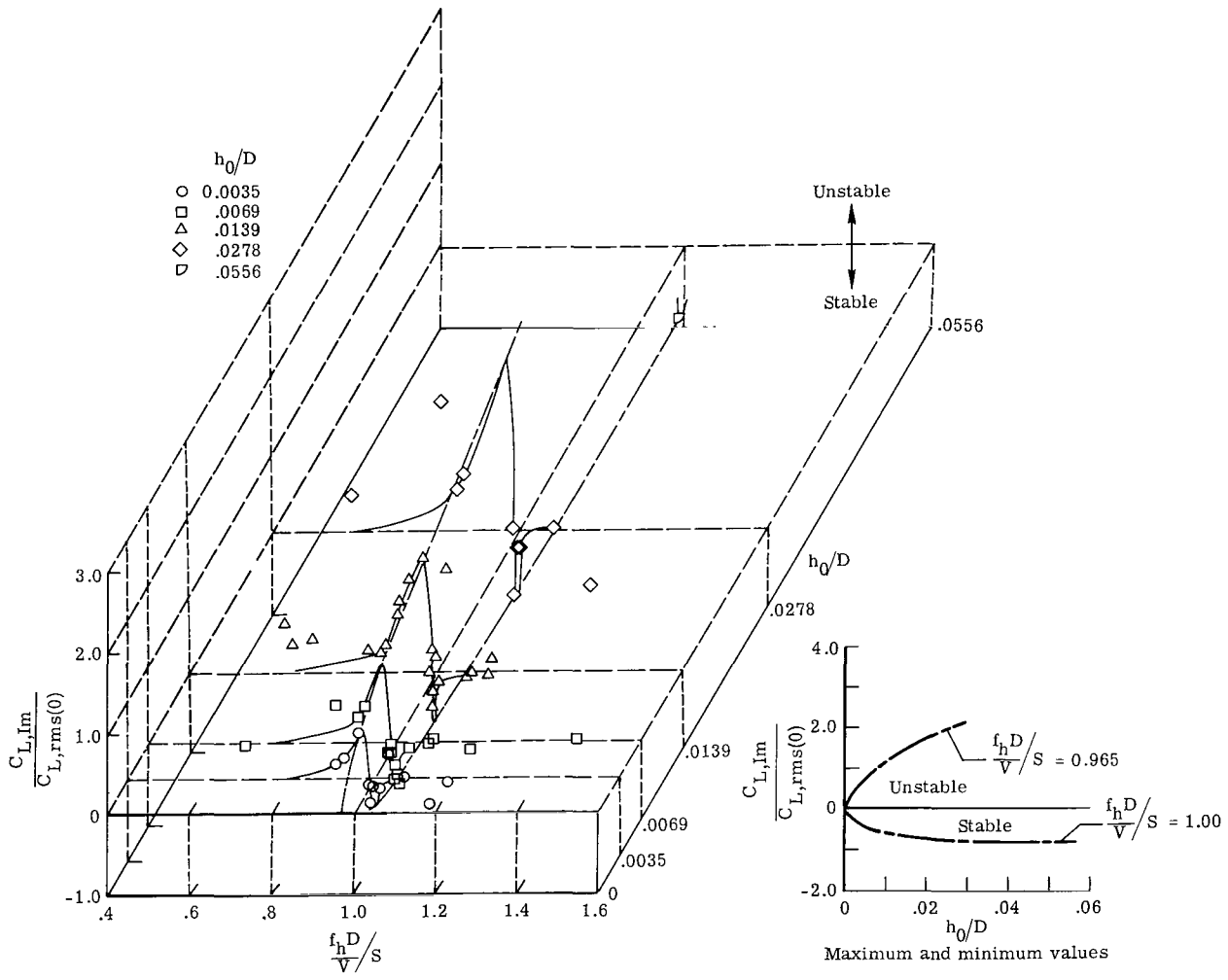

(b) Variation of $\frac{C_{L,Im}}{C_{L,rms(0)}}$ with $\frac{f_h D}{V}/S$ and h_0/D.

Figure 23.- Concluded.

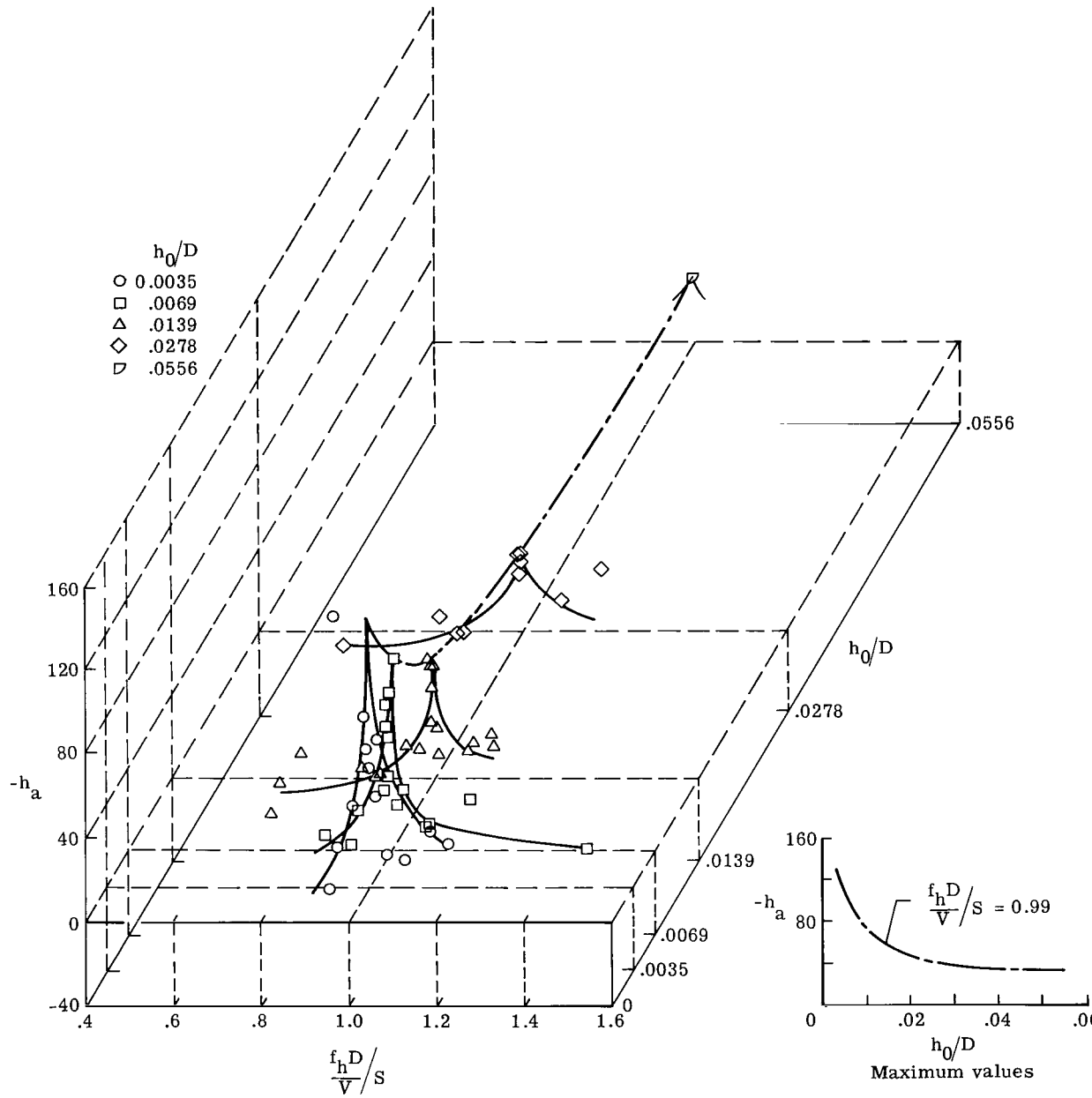

(a) Variation of $-h_a$ with $\frac{f_h D}{V}/S$ and h_0/D.

Figure 24.- Variation of Scruton type aerodynamic derivatives of real and imaginary components of lift coefficient at frequency of cylinder oscillation.

Note: Lift per unit length = $-2S^2qh(h_a + i2\pi k_a)$.

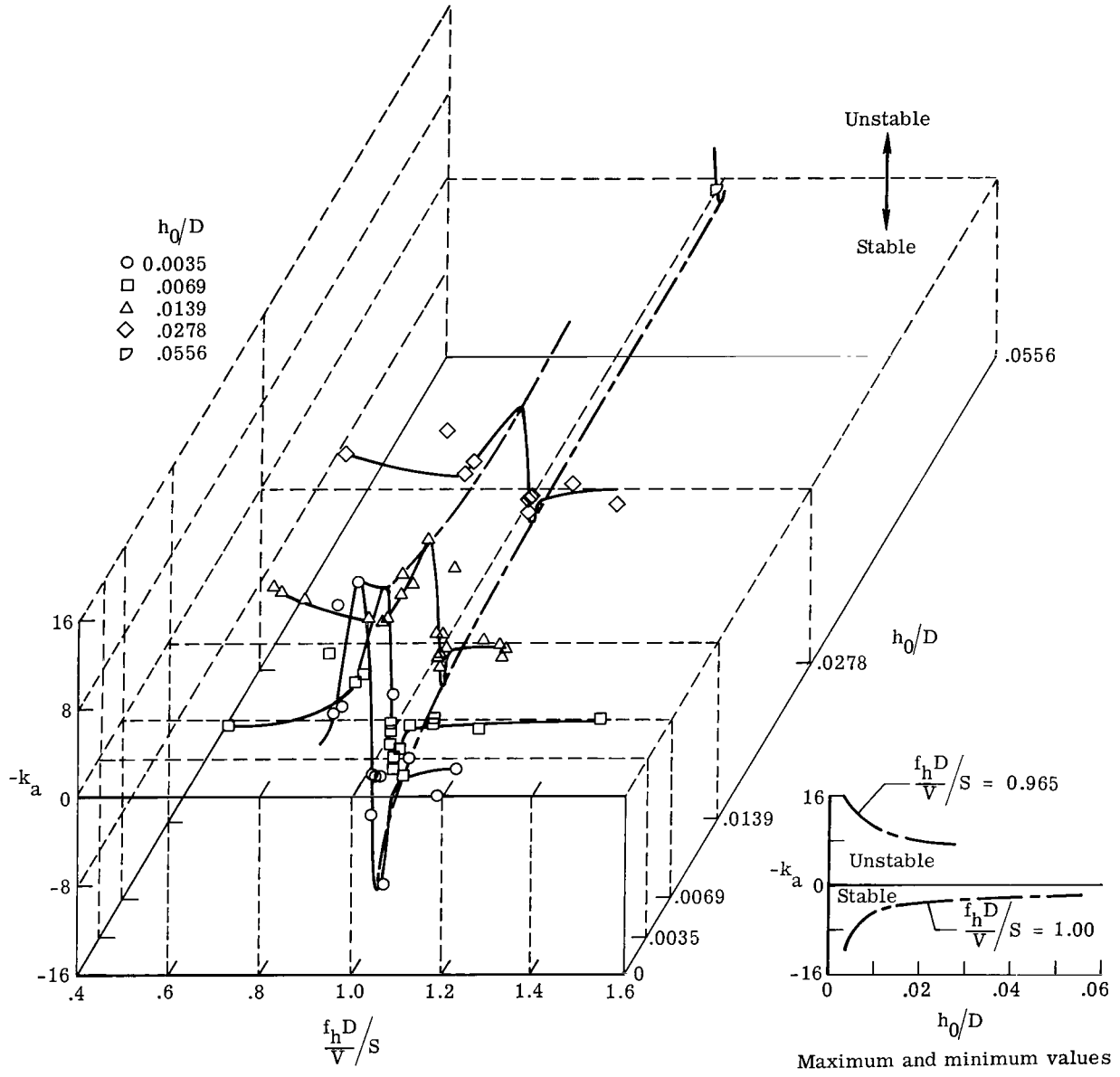

(b) Variation of $-k_a$ with $\frac{f_h D}{V}/S$ and h_0/D.

Figure 24.- Concluded.

inversely with increasing amplitude of motion (as did Scruton's values at lower Reynolds numbers in ref. 4). Thus, there is seen to be a nonlinear aerodynamic damping term in the motion-generated lift force. This damping term occurs at the Strouhal frequency and is inversely proportional to the amplitude of motion. Reed, in reference 15, points out that for actual structures such as a space vehicle erected on the launch pad, a nonlinear aerodynamic damping term can give rise to a limit-amplitude sinusoidal oscillation. An oscillation of this type has been observed on aeroelastic, ground-wind-load models of launch vehicles (ref. 16), and on other structures (ref. 4).

CONCLUSIONS

Analysis of the results of a wind-tunnel study of the mean drag and unsteady lift forces on a stationary and oscillating circular cylinder in two-dimensional flow at high Reynolds numbers indicates the following conclusions:

1. The pressure distributions around the stationary cylinder at Reynolds numbers from 0.5×10^6 to 8×10^6 follow the trends established by previous investigators. At higher (hitherto unexplored) Reynolds numbers from 8×10^6 to 18×10^6, there is no significant change in the pressure distributions.

2. The mean drag coefficient on the stationary cylinder, at Mach numbers equal to or less than about 0.2, follows the trends established by previous investigators at Reynolds numbers from 0.5×10^6 to 8×10^6 and reaches a maximum of 0.54 at a Reynolds number of approximately 3×10^6 and decreases slightly to 0.52 at a Reynolds number of 10×10^6.

3. At Reynolds numbers between 4×10^6 and 8×10^6 and Mach numbers above 0.2, there is a peak in the mean drag coefficient which becomes more pronounced as Mach number is increased from 0.2 to 0.4.

4. Oscillation of the cylinder in the lift direction had no significant effect on the mean drag coefficient.

5. The unsteady lift force on the stationary cylinder can be categorized into three regimes dependent upon Reynolds number R_N as follows: wide-band random ($1.1 \times 10^6 < R_N < 3.5 \times 10^6$), narrow-band random ($3.5 \times 10^6 < R_N < 6.0 \times 10^6$), and quasi-periodic ($6.0 \times 10^6 < R_N < 18.7 \times 10^6$).

6. The Strouhal number of the unsteady lift on the stationary cylinder follows the trends established by previous investigators at Reynolds numbers from about 3×10^6 to 8×10^6. At hitherto unexplored Reynolds numbers from 8×10^6 to 17×10^6, the Strouhal number is approximately constant at a value of about 0.3.

7. At Mach numbers equal to or less than 0.3, the root-mean-square unsteady lift coefficient on the stationary cylinder varies over a wide range at Reynolds numbers from 1.4×10^6 to 8×10^6; then, the range narrows into a single-valued function which decreases slowly with higher Reynolds numbers. At a Mach number of 0.4, the root-mean-square lift coefficient is a single-valued function of Reynolds number with a rounded peak near a Reynolds number of 9×10^6. This peak corresponds roughly to the similar peaks in drag data at this Mach number.

8. A lift force due to cylinder oscillation is found to exist. When the cylinder is oscillated at or near the aerodynamic Strouhal frequency for the stationary cylinder, there is a definite lift due to motion. This lift increases with increasing amplitude of cylinder oscillation building up to values several times the lift on the stationary cylinder. When the cylinder is oscillated at frequencies far removed from the aerodynamic Strouhal frequency of the stationary cylinder, there is no significant lift due to motion.

9. The unsteady lift due to motion of the cylinder has a character such that for motion at frequencies below the aerodynamic Strouhal frequency (vortex-shedding frequency of the stationary cylinder), the unsteady lift is an unstable, negative aerodynamic damping force. Actual flexible cylindrical structures subjected to a negative aerodynamic damping force exhibit a limit-amplitude sinusoidal oscillation. As the frequency of cylinder motion passes through and above the aerodynamic Strouhal frequency of the stationary cylinder, there is an abrupt change in the unsteady lift due to motion to a stable, positive damping force. Aerodynamic derivatives of the components (with respect to displacement) of the unsteady lift due to motion decrease nonlinearly with increasing amplitude of cylinder motion.

Langley Research Center,
National Aeronautics and Space Administration,
Langley Station, Hampton, Va., October 1, 1968,
124-08-04-22-23.

APPENDIX A

ESTIMATION OF SOLID-BLOCKAGE INTERFERENCE

For these tests, the center slots in the floor and ceiling of the test section were closed and the ratio of slotted area to solid area in the vicinity of the model was 0.0414. The size of the cylinder model is large in relation to the size of the test section, the ratio of the model frontal area to the cross-sectional area of the tunnel being 0.193. This ratio is roughly the same as that for the model of reference 5. The data of reference 5 were obtained in a closed tunnel, and corrections for wind-tunnel wall interference were necessary. The data for the present investigation were obtained from a two-dimensional model in a three-dimensional slotted tunnel. Although no theory exists for making wall-interference corrections for this case, it was possible to make an estimate of the solid-blockage interference by using the method of reference 17. For this estimate, the tunnel was assumed to be two-dimensional with four equally spaced, equal-width slots in each side wall, rather than the actual tunnel configuration shown in figure 2. The corrections obtained from this estimate were as follows:

Corrected velocity at model = 0.997 $\times$ Measured free-stream velocity

Corrected mean drag = 1.008 $\times$ Measured mean drag

Since these estimated corrections are less than 1 percent of the measured quantities and since no acceptable theory exists for correcting the unsteady lift on the stationary or oscillating cylinder, no wall-interference corrections have been made to the data of this investigation.

APPENDIX B

DETAILS OF INSTRUMENTATION AND DATA-REDUCTION PROCEDURES

Instrumentation

The Inertia Compensated Balance (ICB) system, as utilized in this study, uses the signals from strain-gage force transducers and from an accelerometer located at the center of the 2.33D-length instrumented section. The summed output of the strain-gage transducers in the lift direction measures both the unsteady aerodynamic forces and the inertia forces induced by model vibration or oscillation. As discussed in reference 18, by subtracting a properly adjusted acceleration signal from the combined force transducer signal, the model inertia loads sensed by the force transducers are compensated so that the unsteady aerodynamic forces can be measured directly. For the cylinder oscillation frequencies of this test (3 to 18.7 hertz), the instrumented cylinder section was effectively rigid so that the model inertia forces were considered to be caused by rigid-body motion only. A circuit schematic diagram of a typical ICB measurement system is shown in figure 25. In addition to the unsteady lift force, the mean drag force on the 2.33D instrumented section was measured by using force transducers oriented in the drag direction and located at the top and bottom of the instrumented cylinder section.

A typical instrumentation block diagram for measuring unsteady lift and steady drag forces and lateral accelerations on the 2.33D cylinder section is presented in figure 26. As shown, the excitation and amplification of the transducers were accomplished by a carrier amplifier system. Amplitude and phase adjusting networks conditioned the signals at the output of the carrier amplifier. The conditioned signals were then appropriately summed in operational amplifiers to produce signals in which inertia components have been effectively eliminated. Significant cross-axis signals were also removed in this summation process.

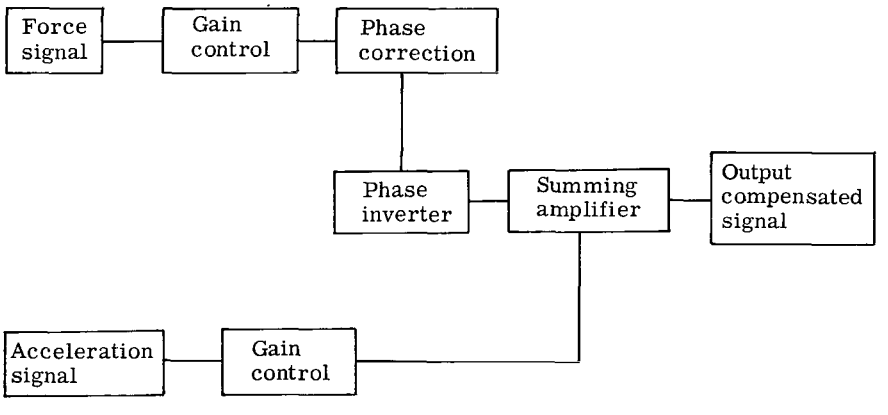

Figure 25.- Circuit schematic diagram of a typical ICB measurement system.

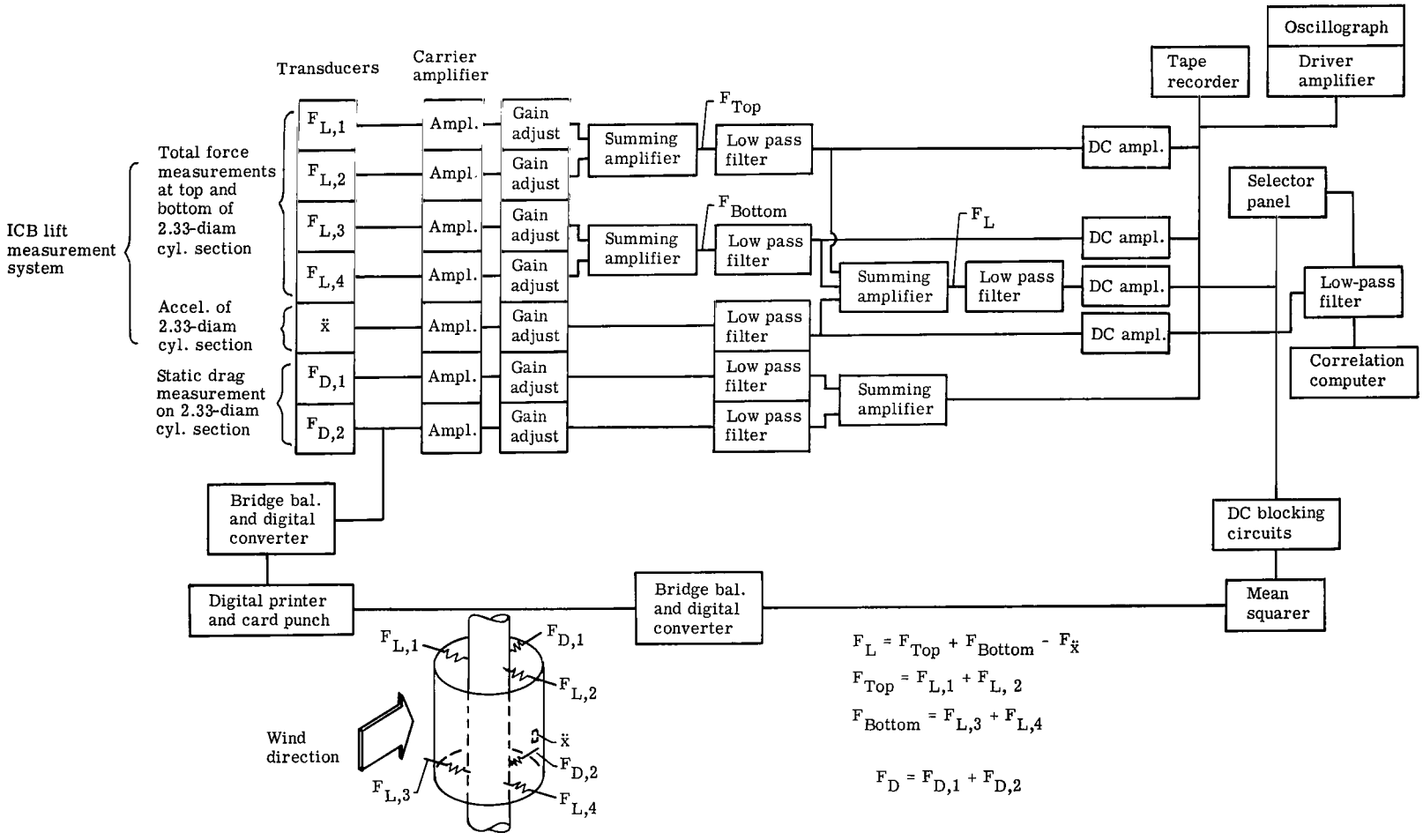

Figure 26.- Instrumentation block diagram for measured aerodynamic forces and acceleration on 2.33D-length instrumented cylinder section.

APPENDIX B

The total and inertia-compensated force signals were amplified and fed to a number of recording and computing devices, including a tape recorder, an oscillograph, a digital mean-square recorder, and "on-line" analysis equipment. (Another recorder handled the measured steady-state values of drag forces prior to reaching the carrier amplifier.) Displacement signals originating in the hydraulic shaker system were also inserted into the recorder and analysis equipment. Signals presented to the mean-square recorder and to the "on-line" analysis equipment were filtered to block the direct-current component and, in addition, were low-pass filtered to remove local model resonance signals above 80 hertz at the mean-square recorder and above 40 hertz at the "on-line" analysis equipment.

Autocorrelation analysis was performed "on-line" by using a hybrid analog-digital computer (ref. 19). This analysis gave a quantitative indication of the random or periodic nature of the force signal. These autocorrelations also gave quantitative information such as the predominant frequency of the unsteady aerodynamic forces.

No attempt was made to measure local-dynamic-pressure fluctuations; however, average-static-pressure distributions were measured during the initial phase of the test program. A ring of 48 static-pressure orifices was installed at one longitudinal station on the model 1.14 diameters from the lower end of the model (test-section floor). The orifices were constructed of monel tubing with an inside diameter of 0.02 inch (0.508 mm) with one end inserted into a plug and flush mounted from the inside of the model to the outside skin. Flexible tubing led from the back of each orifice plug to a multiple-tube manometer board. The manometer board was photographed to obtain simultaneous readings of the 48 static-pressure measurements.

Data-Reduction Procedures

A data-reduction block diagram is presented in figure 27, which shows schematically the types of analyses made of the measured experimental data as recorded on magnetic tape. The analyses shown in the blocks are discussed in the following subsections in terms of the equipment used, the analysis parameters, and the relative accuracy of the reduced data.

Mean square.- The first step in the data analysis was to determine the mean-square value of aerodynamic lift as a function of time by arranging analog equipment to simulate the following equation:

$$\overline{F}_L{}^2(t) = \frac{1}{2T}\int_{t-T}^{t+T} F_L{}^2(t)dt$$

The functional diagram for the mean-square analysis is shown in figure 28. The low-pass filter, which was used to reduce a 60-hertz noise from the signal, was set at a 40 hertz

APPENDIX B

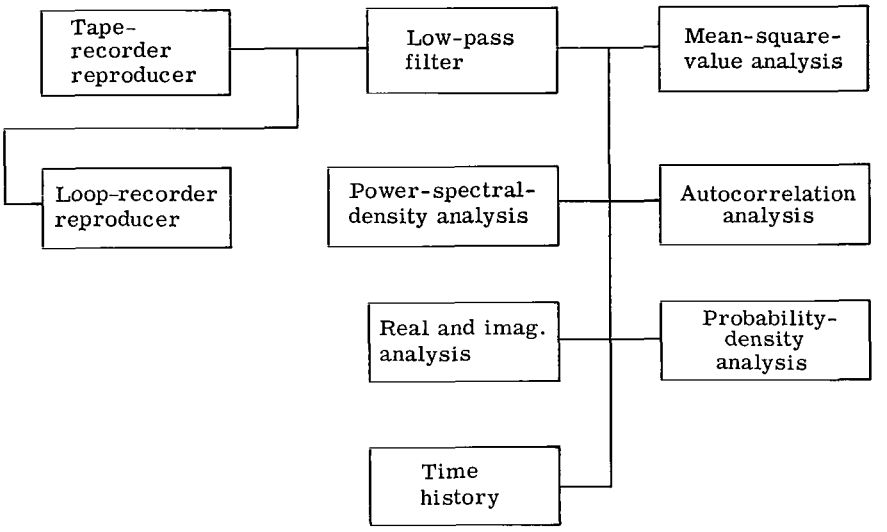

Figure 27.- Data-reduction block diagram.

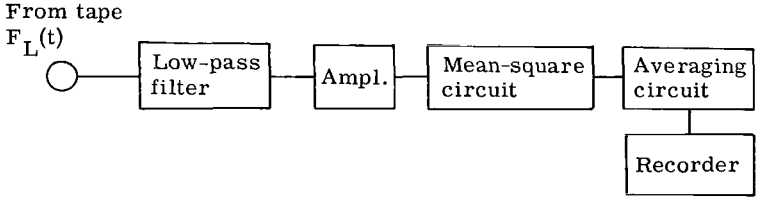

Figure 28.- Functional diagram for mean-square analysis.

cut-off frequency (-3 decibels at 40 hertz, and above 40 hertz the filter cut-off rate was 24 decibels per octave). The filtered signal was amplified with an operational amplifier and sent through the mean-square circuit of a true-mean-square meter. The mean-square output of the meter was then put through an averaging circuit consisting of another operational amplifier that had a time constant of 2.5 seconds. This continuous mean-square value was recorded on a strip chart during the time-history sample period and was once more averaged manually to give a single mean-square value whose square root was taken as the root-mean-square value for the data sample. The accuracy of the analysis equipment used for the mean-square value is within ±12 percent of the measured value.

Power spectral density.- After a review of the mean-square results, tape records of selected data samples were chosen for power-spectral-density analysis. The power spectra were obtained from analog analysis equipment. The functional diagram for the

power-spectral-density analyzer is presented in figure 29. Important real-time parameters for the power-spectral-density analysis were as follows:

Sample length	120 sec
Filter bandwidth	0.41 Hz
Statistical degrees of freedom	98.2
Time constant of averaging circuit	128 sec
Sweep rate	0.025 Hz/sec

All the data samples selected for analyses were re-recorded at a tape speed of $1\frac{7}{8}$ in./sec (4.76 cm/sec). The analyses were performed at 32 times the recorded speed, and a correction factor for the frequency multiplication and bandwidth division was incorporated. The accuracy of the power-spectral-density analysis equipment was generally within ±12 percent in all the test samples where the data bandwidth was greater than four times the filter bandwidth of the analyzer. The indicated frequencies of the analyses were accurate within 0.3 hertz.

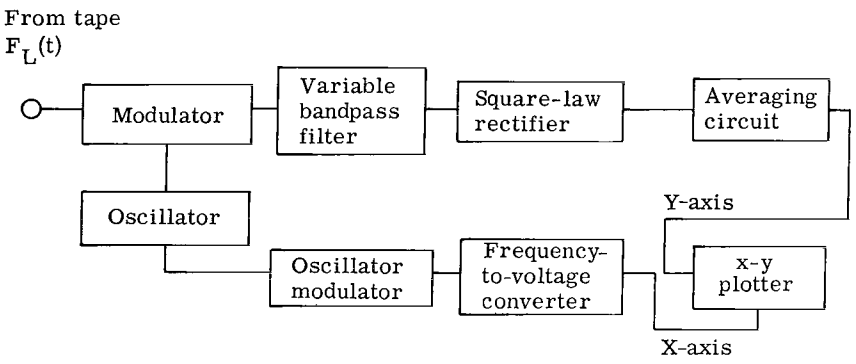

Figure 29.- Functional diagram for power-spectral-density analyzer.

Autocorrelation and probability density.- The nature of the force signal was investigated further by determining the autocorrelation functions and probability densities of the unsteady lift force from the time-history data samples. These functions were computed with the use of the hybrid analog-digital computer.

The autocorrelation analysis performed in the analog-digital computer approximates the following mathematical expression (ref. 20, p. 19) for the autocorrelation function:

$$R(\tau) = \lim_{T \to \infty} \frac{1}{T} \int_0^T F_L(t)\, F_L(t + \tau)dt$$

The approximation is in the form of a summation process where T does not approach infinity but is sufficiently large to enable the quantity under the integral sign, as

displayed graphically on an oscilloscope, to be almost constant, that is, asymptotically approaches a final value. This operation was either performed "on-line" while the time-history data sample was being obtained or after the test from tape records of the time-history data sample of the unsteady lift force F_L.

The same analog-digital computer with an additional attachment was used to calculate the probability density function of the unsteady lift force from tape records of the time-history data samples. The mathematical expression approximated by the computer is given by the following equation (ref. 20, p. 15):

$$p(F_L) = \lim_{\Delta F_L \to 0} \frac{\text{Prob}\left[F_L < F_L(t) < F_L + \Delta F_L\right]}{\Delta F_L} = \lim_{\Delta F_L \to 0} \lim_{T \to \infty} \frac{1}{T}\left(\frac{T_{F_L}}{\Delta F_L}\right)$$

The computer output is displayed on an oscilloscope as $p(F_L)$ plotted against the instantaneous value of F_L.

The instrumentation arrangement for these analyses was to play the lift-force signal at real time through a low-pass filter (40 hertz) and through amplifiers into the hybrid analog-digital computer. The computer performed either the autocorrelation or probability-density analysis and the output of the computer was fed to an x-y plotter which graphed the function. The basic accuracy of the equipment used to obtain these functions was within ±12 percent of the measured value.

Analysis of motion-dependent aerodynamic forces.- In order to gain insight into the basic nature of the unsteady lift due to motion, an analog analysis was made which resolved the unsteady lift force into its fundamental components in phase and 90^o out of phase with displacement. With motion of the cylinder given by $h(t) = h_0 \cos \omega t$, these components are

$$F_{L,Re}(\omega) = \frac{2}{T}\int_0^T F_L(t)\cos \omega t \, dt$$

$$F_{L,Im}(\omega) = \frac{2}{T}\int_0^T F_L(t)\sin \omega t \, dt$$

where ω is the frequency of the cylinder oscillation in radians per second. The functional diagram of the analog analyzer is shown in figure 30. As shown, the lift force and displacement time histories were played from tape through matched amplifiers and matched fixed-band-pass filters (0.02 to 40 hertz). The displacement signal was sent to a tracking oscillator which automatically tracked the displacement frequency ω and generated output signals proportional to $\sin \omega t$ and $\cos \omega t$. The real and imaginary lift-force signals were then multiplied by the $\cos \omega t$ and $\sin \omega t$ signals, respectively, and these products were integrated along the length of the data sample (T = 100 seconds,

APPENDIX B

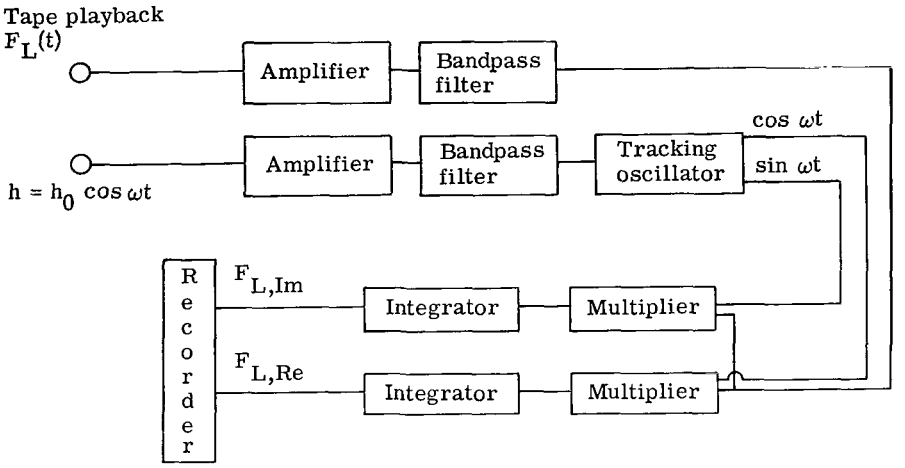

Figure 30.- Functional diagram for analog resolution of lift force at frequency ω into real and imaginary components with respect to displacement.

real time). Thus, any higher harmonic or random components of lift force not at the fundamental frequency of motion of the cylinder would be eliminated from the output by this averaging process. The resulting signals were proportional to the components of lift force that are in phase (real component) and 90° out of phase (imaginary component) with the sinusoidal cylinder motion.

REFERENCES

1. Goldman, R. L.: Karman Vortex Forces on the Vanguard Rocket. Shock Vib. Bull., No. 26, Pt. II, U.S. Dep. Def., Dec. 1958, pp. 171-179.

2. Fung, Y. C.: Fluctuating Lift and Drag Acting on a Cylinder in a Flow at Supercritical Reynolds Numbers. J. Aerosp. Sci., vol. 27, no. 11, Nov. 1960, pp. 801-814.

3. Humphreys, John S.: On a Circular Cylinder in a Steady Wind at Transition Reynolds Numbers. J. Fluid Mech., vol. 9, pt. 4, Dec. 1960, pp. 603-612.

4. Scruton, C.: On the Wind-Excited Oscillations of Stacks, Towers and Masts. Paper 16, Brit. Nat. Phys. Lab., [June 1963].

5. Roshko, Anatol: Experiments on the Flow Past a Circular Cylinder at Very High Reynolds Number. J. Fluid Mech., vol. 10, pt. 3, May 1961, pp. 345-356.

6. Muttray, H.: Die experimentellen Tatsachen des Widerstandes ohne Auftrieb. Handb. Experimentalphys., Bd. IV, 2. Teil, Akad. Verlagsgesellschaft M.B.H. (Leipzig), 1932, p. 316.

7. Schmidt, L. V.: Measurements of Fluctuating Air Loads on a Circular Cylinder. J. Aircraft, vol. 2, no. 1, Jan.-Feb. 1965, pp. 49-55.

8. Schmidt, Louis V.: Fluctuating Force Measurements Upon a Circular Cylinder at Reynolds Numbers up to 5×10^6. NASA paper presented at Meeting on Ground Wind Load Problems in Relation to Launch Vehicles (Langley Research Center), June 7-8, 1966.

9. Relf, E. F.; and Simmons, L. F. G.: The Frequency of the Eddies Generated by the Motion of Circular Cylinders Through a Fluid. R. & M. No. 917, Brit. A.R.C., 1924.

10. Delany, Noel K.; and Sorensen, Norman E.: Low-Speed Drag of Cylinders of Various Shapes. NACA TN 3038, 1953.

11. Bishop, R. E. D.; and Hassan, A. Y.: The Lift and Drag Forces on a Circular Cylinder Oscillating in a Flowing Fluid. Proc. Roy. Soc. (London), ser. A, vol. 277, no. 1368, Jan. 7, 1964, pp. 51-75.

12. Loving, Donald L.; and Katzoff, S.: The Fluorescent-Oil Film Method and Other Techniques for Boundary-Layer Flow Visualization. NASA MEMO 3-17-59L, 1959.

13. Morkovin, M. V.: Flow Around Circular Cylinder – A Kaleidoscope of Challenging Fluid Phenomena. Symposium on Fully Separated Flows, Arthur G. Hansen, ed., Amer. Soc. Mech. Eng., May 18-20, 1964, pp. 102-118.

14. Schlichting, Hermann (J. Kestin, trans.): Boundary Layer Theory. Fourth ed., McGraw-Hill Book Co., Inc., c.1960.

15. Reed, Wilmer H., III: Models for Obtaining Effects of Ground Winds on Space Vehicles Erected on the Launch Pad. The Role of Simulation in Space Technology. Eng. Ext. Ser. Circ. No. 4, Pt. C, Virginia Polytech. Inst., Aug. 1964.

16. Jones, George W., Jr.; and Farmer, Moses G.: Wind-Tunnel Studies of Ground-Wind Loads on Saturn Launch Vehicles. J. Spacecraft Rockets, vol. 4, no. 2, Feb. 1967, pp. 219-223.

17. Davis, Don D., Jr.; and Moore, Dewey: Analytical Study of Blockage- and Lift-Interference Corrections for Slotted Tunnels Obtained by the Substitution of an Equivalent Homogeneous Boundary for the Discrete Slots. NACA RM L53E07b, 1953.

18. Stahle, C. V.; Stouffer, C. G.; and Silver, W.: A Simplified Inertia-Compensated Balance Technique for Wind Tunnel Measurement of Launch Vehicle Random Buffet Excitation. Proceedings of Symposium on Aeroelastic & Dynamic Modeling Technology, RTD-TDR-63-4197, Pt. II, U.S. Air Force, Mar. 1964, pp. 35-62.

19. Saper, Louis M.: On-Line Auto- and Cross-Correlator Realized With Hybrid Computer Techniques. IEEE Int. Conv. Rec., vol. 11, pt. 9, 1963, pp. 120-130.

20. Bendat, Julius S.; and Piersol, Allan G.: Measurement and Analysis of Random Data. John Wiley & Sons, Inc., c.1966.

TABLE I.- MEAN DRAG COEFFICIENT FOR STATIONARY CYLINDER

(a) 2.33D instrumented cylinder section; gaps sealed

C_D	M	R_N	Test medium and pressure
0.493	0.120	2.38×10^6	Air, 1 atm
.567	.167	3.30	
.584	.204	4.03	
.615	.236	4.65	
.634	.264	5.17	
.631	.289	5.66	
.635	.313	6.08	
.702	.342	6.60	
.743	.368	7.05	
.671	.330	6.24	
.500	.119	2.33	
.545	.167	3.27	
.556	.187	3.66	
.547	.204	3.99	
.552	.236	4.62	
.582	.265	5.15	
.632	.296	5.72	
.632	.308	5.94	
.643	.323	6.22	
.655	.333	6.38	
.680	.344	6.55	
.746	.369	6.98	
.795	.377	7.12	
.846	.386	7.25	
.810	.388	7.25	
.384	.086	1.74	
.521	.146	2.92	
.561	.187	3.69	
.603	.221	4.31	
.636	.250	4.86	
.676	.301	5.75	
.725	.353	6.52	
.812	.404	7.33	
.661	.099	4.38	Freon, 1 atm
.567	.130	5.75	
.518	.158	6.97	
.538	.183	8.04	
.526	.208	9.11	
.542	.236	10.33	
.531	.257	11.22	
.558	.275	11.95	
.553	.288	12.44	
.547	.305	13.16	
.558	.329	14.12	
.571	.353	15.10	
0.576	0.356	15.21×10^6	Freon, 1 atm
.583	.366	15.62	
.573	.384	16.26	
.620	.400	16.88	
.617	.416	17.51	
.616	.418	17.57	
.466	.099	4.57	
.463	.139	6.40	
.511	.167	7.67	
.529	.212	9.64	
.534	.276	12.42	
.545	.334	14.86	
.585	.382	16.84	
.627	.418	18.27	
.541	.116	5.12	
.531	.235	10.25	
.550	.306	13.17	
.556	.350	14.96	
.556	.350	14.96	
.580	.364	15.47	
.628	.416	17.55	
.577	.229	10.82	
.597	.186	8.84	
.604	.192	9.11	
.620	.131	6.27	
.521	.138	3.25	Freon, 1/2 atm
.596	.184	4.47	
.566	.237	5.72	
.598	.259	6.22	
.622	.290	6.93	
.613	.316	7.49	
.632	.330	7.82	
.676	.374	8.77	
.688	.385	9.00	
.704	.390	9.10	
.474	.135	3.38	
.490	.185	4.61	
.541	.236	5.66	
.565	.274	6.54	
.583	.303	7.18	
.648	.363	8.49	
.651	.385	8.95	
.693	.410	9.47	
.590	.162	3.92	
.597	.218	5.26	
0.509	0.175	2.95×10^6	Freon, 1/3 atm
.537	.163	2.75	
.532	.164	2.77	
.525	.171	2.89	
.530	.219	3.67	
.557	.231	3.87	
.573	.253	4.22	
.594	.282	4.69	
.622	.291	4.84	
.636	.318	5.26	
.654	.335	5.54	
.676	.350	5.75	
.692	.369	6.04	
.694	.379	6.19	
.700	.383	6.25	
.707	.400	6.38	
.781	.453	7.14	
1.027	.500	7.78	
.588	.187	3.10	
.601	.248	4.10	
.647	.316	5.19	
.631	.315	5.20	
.689	.382	6.21	
.577	.184	2.90	
.591	.246	3.82	
.700	.312	4.81	
.157	.120	.59	Freon, 1/10 atm
.208	.173	.84	
.228	.217	1.05	
.277	.257	1.24	
.318	.284	1.36	
.363	.320	1.53	
.402	.344	1.63	
.495	.371	1.75	
.535	.386	1.82	
.543	.421	1.96	
.509	.401	1.90	
.422	.288	1.41	
.642	.413	2.08	
.718	.457	2.29	
1.266	.510	2.59	
1.545	.553	2.77	
1.856	.603	3.02	

TABLE I.- MEAN DRAG COEFFICIENT FOR STATIONARY CYLINDER – Concluded

(b) 2.33D instrumented cylinder section; gaps open

C_D	M	R_N	Test medium and pressure
0.489	0.054	1.08×10^6	Air, 1 atm
.553	.088	1.77	
.579	.135	2.68	
.645	.178	3.49	
.654	.226	4.35	
.704	.291	5.51	
.637	.183	3.58	
.623	.212	4.12	
.638	.152	2.96	
.673	.273	5.27	
.593	.181	3.54	
.625	.229	4.41	
.694	.288	5.44	
.802	.389	7.06	
.715	.067	.66	Air, 1/2 atm
.628	.158	1.54	
.617	.208	2.03	
.632	.260	2.54	
.647	.329	3.23	
.606	.132	1.31	
.729	.356	3.54	
.731	.319	3.18	
.626	.206	.36	Air, 1/10 atm
.678	.293	.52	
.727	.344	.60	
.747	.469	.80	
.687	.411	.73	
.626	.117	5.44	Freon, 1 atm
.553	.154	7.17	
.557	.421	18.70	
.549	.206	9.58	
.570	.264	12.15	
.573	.309	14.08	
.612	.370	16.66	
.633	.397	17.82	

(c) Integrated pressure distribution; gaps open

c_d	c_l	M	R_N	Test medium and pressure
0.518	-0.020	0.054	1.08×10^6	Air, 1 atm
.537	.021	.088	1.77	
.559	-.126	.135	2.68	
.583	-.257	.178	3.49	
.650	-.083	.226	4.35	
.605	-.016	.351	6.51	
.576	-.097	.183	3.58	
.598	-.040	.212	4.12	
.627	.005	.278	5.33	
.559	.026	.152	2.96	
.584	-.062	.273	5.27	
.563	.003	.067	.66	Air, 1/2 atm
.542	.106	.158	1.54	
.539	.074	.208	2.03	
.590	.051	.260	2.54	
.594	-.159	.329	3.23	
.541	.183	.132	1.31	
.602	-.191	.354	3.55	
.644	-.171	.390	3.90	
.594	-.184	.319	3.18	
.570	.064	.206	.36	Air, 1/10 atm
.623	.064	.293	.52	
.648	.111	.344	.60	
.683	.062	.469	.80	
.688	.092	.411	.73	
.532	-.004	.177	8.27	Freon, 1 atm
.536	.000	.309	14.08	
.584	-.013	.117	5.44	
.543	-.003	.154	7.17	
----	-----	.421	18.70	
.509	-.011	.206	9.58	
.522	-.006	.264	12.15	
.566	-.006	.370	16.66	
.593	-.008	.397	17.82	

TABLE II.- C_D AND R_N VALUES AT CONSTANT MACH NUMBER FOR 2.33D INSTRUMENTED CYLINDER WITH GAPS SEALED

[From cross plots of data of table I(a)]

M	Air, 1 atm		Freon, 1 atm		Freon, $\frac{1}{2}$ atm		Freon, $\frac{1}{3}$ atm		Freon, $\frac{1}{10}$ atm	
	C_D	R_N	C_D	R_N	C_D	R_N	C_D	R_N	C_D	R_N
0.10	0.452	1.97×10^6	0.538	4.45×10^6	----	----------	----	----------	0.143	0.490×10^6
	.472	1.95	.494	4.65	----	----------	----	----------	----	----------
	.420	2.00	----	----------	----	----------	----	----------	----	----------
0.15	0.543	2.96×10^6	0.535	6.60×10^6	0.549	3.64×10^6	0.520	2.54×10^6	0.184	0.725×10^6
	.534	2.93	.499	6.88	.490	3.88	----	----------	----	----------
	.527	2.97	.540	6.55	----	----------	----	----------	----	----------
0.20	0.591	3.95×10^6	0.535	8.76×10^6	0.583	4.83×10^6	0.540	3.36×10^6	0.218	0.962×10^6
	.540	3.91	.505	9.09	.521	4.91	.590	3.30	----	----------
	.589	3.95	.540	8.73	.595	4.83	.587	3.14	----	----------
0.25	0.621	4.92×10^6	0.540	10.92×10^6	0.599	6.02×10^6	0.575	4.17×10^6	0.270	1.20×10^6
	.570	4.87	.524	11.30	.552	5.98	.610	4.13	----	----------
	.630	4.86	.546	10.87	----	----------	.609	3.92	----	----------
0.30	0.632	5.84×10^6	0.550	12.97×10^6	0.613	7.15×10^6	0.619	4.97×10^6	0.338	1.44×10^6
	.611	5.80	.535	13.47	.583	7.11	.634	4.94	.431	1.46
	.669	5.70	.553	12.93	----	----------	.641	4.63	----	----------
0.35	0.723	6.74×10^6	0.570	14.96×10^6	0.650	8.23×10^6	0.671	5.75×10^6	0.420	1.66×10^6
	.700	6.66	.563	15.54	.621	8.20	.670	5.73	.464	1.67
	.727	6.48	.573	14.92	----	----------	----	----------	----	----------
0.40	----	----------	0.608	16.88×10^6	0.628	9.31×10^6	0.730	6.50×10^6	0.549	1.88×10^6
	0.900	7.47×10^6	.608	17.54	.680	9.25	.711	6.39	.500	1.87
	.803	7.27	.608	16.91	----	----------	----	----------	----	----------
0.45	----	----------	----	----------	----	----------	0.781	7.18×10^6	0.764	2.27×10^6
0.50	----	----------	----	----------	----	----------	1.028	7.75×10^6	1.184	2.53×10^6
0.55	----	----------	----	----------	----	----------	----	----------	1.530	2.78×10^6
0.60	----	----------	----	----------	----	----------	----	----------	1.819	3.00×10^6

TABLE III.- STROUHAL NUMBER OF UNSTEADY LIFT ON STATIONARY CYLINDER

[From cross plots of data of table IV]

M	Air, 1 atm		Freon, 1 atm		Freon, $\frac{1}{2}$ atm		Freon, $\frac{1}{3}$ atm		Freon, $\frac{1}{10}$ atm	
	S	R_N	S	R_N	S	R_N	S	R_N	S	R_N
0.10	----	---------	0.233	4.23×10^6	----	---------	----	---------	----	---------
.15	0.217	2.96×10^6	.303	6.89	0.214	3.86×10^6	----	---------	----	---------
.20	.238	3.88	.306	9.10	.251	4.95	0.177	3.14×10^6	----	---------
.25	.243	4.79	.305	11.27	.283	6.06	.206	3.97	----	---------
.30	.251	5.65	.301	13.35	.300	7.17	.232	4.80	0.182	1.38×10^6
.35	.252	6.48	.295	15.40	.305	8.21	.253	5.61	.187	1.66
.40	.251	7.20	.287	17.48	.294	9.25	.267	6.38	.192	1.95
.45	----	---------	----	----------	----	---------	.270	7.15	.199	2.20
.50	----	---------	----	----------	----	---------	.257	7.81	.207	2.47

TABLE IV.- ROOT-MEAN-SQUARE LIFT COEFFICIENT ON STATIONARY CYLINDER

[From autocorrelation functions]

R_N	M	V		q		Test medium and pressure	Nature of unsteady lift force (a)	S (b)	$C_{L,rms(0)}$ (c)
		ft/sec	m/sec	psf	N/m^2				
1.73×10^6	0.086	----	-----	10.9	521.9	Air, 1 atm	WB	----	0.0628
2.91	.147	167.1	50.93	31.3	1 498.7		WB	0.214	.1001
3.69	.187	213.5	65.07	50.7	2 427.5		WB	.237	.1250
4.31	.221	252.7	77.02	70.0	3 351.6		NB	.241	.1420
4.55	.251	287.8	87.72	89.5	4 285.3		NB	.243	.1510
5.75	.303	348.1	106.10	128.0	6 128.7		NB	.247	.1180
6.54	.353	407.1	124.08	170.0	8 139.6		NB	.251	.0863
7.23	.404	468.4	142.77	217.0	10 390.0		NB	.251	.0489
3.30	.130	64.3	19.60	9.6	459.7	Freon, 1/2 atm	WB	----	.0705
4.74	.185	92.5	28.19	19.7	943.2		NB	.243	.1080
5.76	.227	113.7	34.66	29.5	1 412.5		NB	.269	.0893
5.61	.234	118.0	35.97	30.0	1 436.4		NB	.258	.0929
6.51	.273	138.6	42.24	41.1	1 967.9		QP	.293	.0906
7.20	.304	154.5	47.09	50.6	2 422.7		QP	.299	.0918
8.49	.363	184.3	56.17	71.5	3 423.4		QP	.302	.1222
8.94	.385	196.0	59.74	80.2	3 840.0		QP	.294	.1609
9.45	.410	209.0	63.70	90.3	4 323.6		QP	.290	.1768
9.48	.408	----	----	91.0	4 357.1		QP	.289	.2086
4.48	.097	49.7	15.15	10.2	488.4	Freon, 1 atm	WB	.234	.1045
6.36	.137	69.6	21.21	20.3	972.0		QP	.295	.0943
7.66	.166	84.1	25.63	29.6	1 417.3		QP	.308	.0932
9.63	.211	107.0	32.61	47.4	2 269.5		QP	.305	.0618
12.42	.270	138.0	42.06	78.7	3 768.2		QP	.299	.0534
14.93	.330	170.3	51.91	117.3	5 616.4		QP	.294	.0516
16.82	.380	193.8	59.07	150.7	7 215.6		QP	.291	.0921
18.20	.410	211.4	64.43	177.5	8 498.7		QP	.289	.0937
9.33	.200	102.6	31.27	43.8	2 097.2		QP	.314	.0575
11.88	.262	133.1	40.57	73.1	3 500.0		QP	.302	.0565
15.76	.350	179.3	54.65	129.5	6 200.5		QP	.294	.0516
16.82	.380	193.5	58.98	150.2	7 191.6		QP	.292	.0862
7.61	.160	84.2	25.66	29.6	1 417.3		QP	.313	.0815
6.38	.400	204.7	62.39	60.2	2 882.4	Freon, 1/3 atm	QP	.255	.0945
7.11	.450	232.1	70.74	76.3	3 653.3		QP	.269	.1278

[a]The abbreviations used in this column are defined as follows:

WB – Wide-band random (autocorrelation function is described by no more than one peak other than the $\tau = 0$ peak)

NB – Narrow-band random (autocorrelation function consists of more than two consecutive peaks and decreasing amplitudes, with increasing τ-displacement, of more than 10 percent)

QP – Quasi-periodic (autocorrelation function described by consistent peaks through entire analysis – τ-displacement range with constant amplitude within 10 percent at the largest τ-displacement peaks)

[b]Determined from autocorrelation function of the large cylinder aerodynamic lift force.

[c]Lift coefficient determined from the lift force $\tau = 0$ point of the autocorrelation functions.

TABLE IV.- ROOT-MEAN-SQUARE LIFT COEFFICIENT ON STATIONARY CYLINDER – Concluded

R_N	M	V		q		Test medium and pressure	Nature of unsteady lift force (a)	S (b)	$C_{L,rms(0)}$ (c)
		ft/sec	m/sec	psf	N/m^2				
7.79×10^6	0.500	255.6	77.91	91.8	4 395.4	Freon, 1/3 atm	QP	0.248	0.3668
3.06	.180	95.3	29.05	13.6	651.2		WB	----	.0839
4.16	.250	129.5	39.47	25.0	1 197.0		WB	.226	.1372
5.18	.316	162.9	49.65	39.2	1 876.9		NB	.255	.1140
5.18	.314	162.1	49.41	38.9	1 862.5		NB	.233	.1167
6.19	.381	196.2	59.80	56.5	2 705.2		NB	.265	.0932
5.17	.116	59.7	18.20	14.5	694.3		NB	.255	.0698
6.08	.138	71.6	21.82	20.8	995.9		QP	.299	.0788
8.43	.193	99.7	30.39	40.1	1 920.0		QP	.304	.0764
10.23	.234	121.6	37.06	59.3	2 839.3		QP	.303	.0645
13.23	.307	160.0	48.77	101.5	4 859.8		QP	.294	.0495
14.94	.350	181.4	55.29	129.5	6 200.5		QP	.298	.0560
15.48	.364	189.6	57.79	140.7	6 736.8		QP	.295	.0710
17.60	.417	216.8	66.08	182.4	8 733.4		QP	.280	.0900
4.98	.112	58.4	17.80	13.9	665.5		NB	.249	.0760
3.90	.161	84.8	25.85	15.4	737.4	Freon, 1/2 atm	WB	.221	.1179
5.31	.220	115.2	35.11	29.4	1 407.7		NB	.267	.0760
1.88	.399	206.8	63.03	17.8	852.3	Freon, 1/10 atm	NB	.192	.0918
1.42	.293	151.3	46.12	10.0	478.8		WB	.180	.0585
2.09	.415	212.0	64.62	20.0	957.6		WB	.200	.0711
2.30	.460	235.3	71.72	24.5	1 173.1		NB	.203	.0868
2.57	.506	259.0	78.94	30.2	1 446.0		QP	.205	.7039
2.79	.553	284.2	86.62	36.2	1 733.3		QP	.221	.7163
3.01	.601	308.6	94.06	42.3	2 025.3		QP	.229	.6602
2.53	.157	81.8	24.93	9.7	464.4	Freon, 1/3 atm	WB	----	.0902
2.97	.187	96.9	29.54	13.5	646.4		WB	.175	.1062
3.82	.256	128.4	39.14	23.3	1 115.6		NB	.173	.1429
4.90	.318	160.2	48.83	38.6	1 848.2		NB	.226	.1295
10.83	.229	116.1	35.39	58.1	2 781.8	Freon, 1 atm	QP	.301	.0339
8.87	.186	94.8	28.90	39.1	1 872.1		QP	.308	.0770
9.15	.192	98.0	29.87	41.7	1 996.6		QP	.306	.0665
5.32	.110	56.6	17.25	14.0	670.3		NB	.255	.0710
6.17	.129	65.6	20.00	18.8	900.1		QP	.307	.0578

[a]The abbreviations used in this column are defined as follows:

WB – Wide-band random (autocorrelation function is described by no more than one peak other than the $\tau = 0$ peak)

NB – Narrow-band random (autocorrelation function consists of more than two consecutive peaks and decreasing amplitudes, with increasing τ-displacement, of more than 10 percent)

QP – Quasi-periodic (autocorrelation function described by consistent peaks through entire analysis – τ-displacement range with constant amplitude within 10 percent at the largest τ-displacement peaks)

[b]Determined from autocorrelation function of the large cylinder aerodynamic lift force.

[c]Lift coefficient determined from the lift force $\tau = 0$ point of the autocorrelation functions.

TABLE V.- REDUCED DATA FOR UNSTEADY LIFT ON OSCILLATING TWO-DIMENSIONAL CYLINDER

R_N	M	h_0/D (nominal)	$\frac{f_h D}{V}/S$	$\frac{C_{L,rms(h/D)}}{C_{L,rms(0)}}$	$\lvert C_L \rvert$	θ, deg	$\frac{C_{L,Re}}{C_{L,rms(0)}}$	$\frac{C_{L,Im}}{C_{L,rms(0)}}$	$-h_a$	$-k_a$	$(h_0/D)_{rms}$	$\frac{f_h D}{V}$	S	$C_{L,rms(0)}$	$C_{L,rms(h/D)}$	$C_{L,Re}$	$C_{L,Im}$	V ft/sec	V m/sec	q psf	q N/m^2
6.15×10^6	0.379	0.0035	0.958	1.190	0.0454	68.5	0.2207	0.5625	39.21	15.903	0.0033	0.253	0.264	0.0895	0.0752	0.0166	0.0423	195.4	59.56	56.0	2681.3
6.17	.129		1.031	.799	.0235	67.0	.1223	.2872	15.91	5.944	.0033	.297	.288	.0601	.0752	.0092	.0216	65.6	19.99	18.8	900.1
6.24	.130		1.177	.776	.0164	-15.6	.2101	-.0585	20.97	-.9296	.0033	.339	.288	.0584	.0752	.0158	-.0044	66.3	20.21	19.2	919.3
8.49	.360		.917	1.465	.0804	33.8	.9214	.6165	129.57	13.799	.0034	.277	.302	.1062	.0725	.0668	.0447	183.9	56.05	71.8	3437.8
9.15	.192		.984	1.013	.0467	4.5	.6563	-.0721	81.40	-1.424	.0032	.300	.305	.0716	.0707	.0464	-.0051	98.0	29.87	41.7	1996.6
9.15	.192		.905	.992	.0137	91.7	-.0056	.1938	-.76	4.158	.0034	.276	.305	.0701	.0707	-.0004	.0137	98.0	29.87	41.7	1996.6
10.24	.234		.987	1.106	.0433	-26.2	.5894	-.2894	66.05	-5.162	.0032	.301	.305	.0730	.0660	.0389	-.0191	121.6	37.06	59.4	2844.1
10.74	.227		1.010	.950	.0286	-12.9	.4387	-.1006	43.67	-1.594	.0034	.308	.305	.0604	.0636	.0279	-.0064	113.8	34.69	55.8	2671.7
10.81	.229		1.072	.918	.0095	.8	.1498	.0016	13.15	.0220	.0034	.327	.305	.0582	.0634	.0095	.0001	116.7	35.57	58.6	2805.8
10.85	.230		.924	.963	.0190	-4.8	2.960	-.2488	19.65	4.705	.0034	.282	.305	.0607	.0630	.0105	.0158	117.0	35.66	58.9	2820.1
11.97	.26		.997	1.106	.0303	-9.4	.5227	-.0857	57.07	-1.488	.0028	.304	.305	.0633	.0572	.0299	-.0049	133.4	40.66	73.3	3509.6
13.17	.306		1.133	1.084	.0269	-37.2	4.196	-.3196	27.32	-3.312	.0034	.340	.300	.0553	.0510	.0214	-.0163	159.0	48.46	100.1	4792.8
15.8	.35		1.014	----	.0428	-45.5	-----	-----	70.22	-11.40	.0024	.299	.295	.0635	-----	.0300	-.0306	179.4	54.68	130.1	6229.2
5.67	.237	.0069	.629	1.188	.0144	-6.2	.1915	-.0213	36.71	-.649	.0066	.173	.275	.0893	.0752	.0144	-.0016	121.2	36.94	31.7	1517.8
6.0	.136		1.027	.936	.0330	-7.5	.4348	-.0572	28.49	-.596	.0062	.303	.295	.0704	.0752	.0327	-.0043	70.4	21.46	20.1	962.4
6.0	.136		1.444	.902	.0049	36.2	.0519	.0386	1.68	.198	.0064	.426	.295	.0678	.0752	.0039	.0029	70.4	21.46	20.1	962.4
6.24	.130		1.177	.791	.0377	-12.6	.4894	-.1090	24.02	-.852	.0067	.339	.288	.0595	.0752	.0368	-.0082	66.3	20.21	19.2	919.3
7.21	.303		1.003	1.432	.0823	-9.8	1.084	-.1872	91.58	-2.516	.0049	.301	.300	.1071	.0748	.0811	-.0140	154.5	47.09	51.2	2451.5
7.56	.16		1.010	1.151	.0469	-55.2	.3617	-.5196	21.87	-5.000	.0064	.309	.306	.0853	.0741	.0268	-.0385	84.4	25.72	29.5	1412.5
8.4	.190		.990	1.078	.0503	-38.6	.5391	-.4307	34.34	-4.367	.0063	.302	.305	.0786	.0729	.0393	-.0314	99.2	30.24	39.6	1896.0
9.15	.192		.984	1.173	.0743	1.3	1.051	-.0212	69.12	-.222	.0060	.300	.305	.0829	.0707	.0743	-.0015	98.0	29.87	41.7	1996.6
9.15	.192		.905	.986	.0216	84.3	.0297	.3041	2.08	3.397	.0066	.276	.305	.0697	.0707	.0021	.0215	98.0	29.87	41.7	1996.6
9.16	.193		1.082	.982	.0194	2.9	.2748	.0142	13.36	.110	.0067	.330	.305	.0693	.0706	.0194	.0010	98.3	29.96	41.8	2001.4
9.3	.20		.849	.911	.0332	79.1	.0900	.4657	7.22	5.948	.0065	.259	.305	.0638	.0700	.0063	.0326	104.2	31.76	45.1	2159.4
9.51	.41		.741	----	-----	----	------	-----	-----	-------	-----	.215	.290	-----	.0692	-----	-----	209.2	63.76	91.6	4385.8
10.17	.233		.987	1.196	.0739	-20.2	1.048	-.3852	58.92	-3.446	.0065	.301	.305	.0792	.0662	.0694	-.0255	121.5	37.03	59.0	2824.9
10.74	.228		1.079	.997	.0183	-5.5	.2862	-.0283	11.54	-.182	.0073	.329	.305	.0634	.0636	.0182	-.0018	115.9	35.33	57.8	2767.5
10.77	.228		.993	1.211	.0708	-14.7	1.079	-.2835	53.15	-2.223	.0070	.303	.305	.0769	.0635	.0685	-.0180	115.8	35.30	57.7	2762.7
10.86	.231		.921	.976	.0355	53.2	.3386	.4515	19.67	4.172	.0069	.281	.305	.0614	.0629	.0213	.0284	117.5	35.81	59.4	2844.1
11.96	.26		.984	1.013	.0306	-11.9	.5227	-.1101	28.69	-.962	.0056	.304	.309	.0631	.0572	.0299	-.0063	133.4	40.66	73.2	3504.8
13.14	.304		.993	1.660	.0968	3.9	1.887	-.1289	74.31	-.808	.0073	.298	.300	.0850	.0512	.0966	-.0066	156.9	47.82	99.6	4768.9
5.64	.235	.0139	.909	1.402	.0653	100.4	-.1569	.8537	-7.07	6.118	.0134	.250	.275	.1054	.0752	-.0118	.0642	119.7	36.48	31.0	1484.3
5.67	.236		.964	1.523	.1080	76.7	.3297	1.397	13.66	9.163	.0130	.265	.275	.1145	.0752	.0248	.1051	120.2	36.64	31.3	1498.6
5.72	.303		.314	1.162	.0017	----	-.0199	-.0106	-8.60	-.730	.0118	.086	.274	.0874	.0752	-.0015	-.0008	348.1	106.10	128.0	6128.7
5.97	.135		.871	.905	.0246	100.6	.0598	.3218	2.59	2.214	.0132	.257	.295	.0681	.0752	.0045	.0242	70.1	21.37	20.0	957.6
6.00	.130		.831	.725	.0217	72.8	.0851	.2752	4.09	2.105	.0135	.241	.290	.0617	.0752	.0064	.0207	66.1	20.15	18.0	861.8
6.06	.130		1.128	1.150	.0634	-2.3	.8431	-.0332	20.84	-.131	.0142	.327	.290	.0865	.0752	.0634	-.0025	66.1	20.15	18.3	876.2

TABLE V.- REDUCED DATA FOR UNSTEADY LIFT ON OSCILLATING TWO-DIMENSIONAL CYLINDER – Concluded

R_N	M	h_0/D (nominal)	$\frac{f_h D}{V}/S$	$\frac{C_{L,rms(h/D)}}{C_{L,rms(0)}}$	$\lvert C_L \rvert$	θ, deg	$\frac{C_{L,Re}}{C_{L,rms(0)}}$	$\frac{C_{L,Im}}{C_{L,rms(0)}}$	$-h_a$	$-k_a$	$(h_0/D)_{rms}$	$\frac{f_h D}{V}$	S	$C_{L,rms(0)}$	$C_{L,rms(h/D)}$	$C_{L,Re}$	$C_{L,Im}$	V		q	
																		ft/sec	m/sec	psf	N/m^2
6.14×10^6	0.378	0.0139	0.580	----	-----	----	-----	-----	------	------	-----	0.153	0.264	-----	0.0752	-----	-----	195.5	59.59	55.9	2676.5
6.24	.130	|	1.021	1.229	0.0992	75.7	0.3243	1.278	10.68	6.692	0.0132	.294	.288	0.0924	.0752	0.0244	0.0961	66.3	20.21	19.2	919.3
6.24	.130	|	.864	.766	.0175	89.6	.0013	.2327	.06	1.685	.0133	.249	.288	.0576	.0752	.0001	.0175	66.3	20.21	19.2	919.3
7.21	.303	|	.647	1.297	.0264	172.6	-.0454	.3502	-3.598	4.412	.0126	.194	.300	.0970	.0748	-.0034	.0262	154.6	47.12	51.2	2451.5
7.60	.16	|	.696	1.180	.0327	65.4	.1838	.4014	11.39	3.957	.0132	.213	.306	.0873	.0740	.0136	.0297	84.4	25.72	29.7	1422.0
7.62	.16	|	1.006	1.224	.0614	-43.2	.8203	-.1230	23.90	-5.70	.0134	.308	.306	.0906	.0740	.0607	-.0091	84.7	25.82	29.8	1426.8
7.9	.16	|	1.134	1.220	.0489	14.4	.6414	.1651	14.85	.608	.0132	.347	.306	.0902	.0739	.0474	.0122	86.3	26.30	30.9	1479.5
8.4	.192	|	.990	1.034	.0663	-28.7	.7984	-.4362	26.32	-2.289	.0121	.302	.305	.0754	.0729	.0582	-.0318	99.5	30.33	39.9	1910.4
9.15	.192	|	.984	1.629	.1369	-1.1	1.936	.0184	56.34	.0851	.0135	.300	.305	.1152	.0707	.1369	.0013	98.0	29.87	41.7	1996.6
9.15	.192	|	.905	1.027	.0523	86.2	.0481	.7383	1.67	4.090	.0133	.276	.305	.0726	.0707	.0034	.0522	98.0	29.87	41.7	1996.6
9.15	.192	|	1.088	1.098	.0481	.5	.6803	.0056	16.33	.0216	.0134	.332	.305	.0776	.0707	.0481	.0004	98.0	29.87	41.7	1996.6
9.30	.20	|	.997	1.673	.1369	5.5	1.947	.1857	53.09	.806	.0139	.304	.305	.1171	.0700	.1363	.0130	103.5	31.55	44.5	2130.7
10.17	.233	|	.987	1.644	.1239	-8.6	1.852	.2779	53.82	-1.286	.0126	.301	.305	.1088	.0662	.1226	-.0184	121.5	37.03	59.0	2824.9
10.74	.228	|	.931	1.186	.0815	64.8	.5456	1.159	15.31	5.175	.0140	.284	.305	.0754	.0636	.0347	.0737	116.0	35.36	57.8	2767.5
10.74	.229	|	1.072	.860	.0380	6.2	.5123	-.0695	13.02	-.2811	.0135	.327	.305	.0631	.0734	.0376	-.0051	116.5	35.51	58.6	2805.8
10.80	.229	|	.990	1.507	.1084	-8.1	1.697	-.2401	42.96	-.968	.0137	.302	.305	.0954	.0633	.1074	-.0152	116.3	35.45	58.2	2786.6
13.23	.307	↓	.627	.996	.0346	117.8	-.3163	.6012	-16.75	5.067	.0136	.188	.300	.0507	.0509	-.0161	.0306	160.0	48.77	101.5	4859.8
6.11	.139	.0278	.847	1.013	.0403	93.6	-.0332	.5346	-.544	1.393	.0264	.250	.295	.0762	.0752	-.0025	.0402	72.1	21.98	21.1	1010.3
6.24	.130	|	.864	.922	.0536	92.2	-.0266	.7128	-.59	2.538	.0271	.249	.288	.0693	.0752	-.0020	.0536	66.3	20.21	19.2	919.3
6.24	.130	|	1.177	1.914	.1782	-17.1	2.266	-.6942	29.63	-1.445	.0250	.339	.288	.1439	.0752	.1704	.0522	66.3	20.21	19.2	919.3
8.40	.192	|	.987	1.712	.1343	-26.0	1.656	-.8080	26.33	-2.045	.0253	.301	.305	.1248	.0729	.1207	-.0589	99.6	30.36	40.0	1915.2
8.46	.193	|	.587	1.137	.0352	107.9	-.1484	.4602	-6.57	3.242	.0256	.179	.305	.0828	.0728	-.0108	.0335	100.4	30.60	40.6	1943.9
9.15	.192	|	.984	2.112	.1850	28.8	2.574	-.4653	37.60	-1.082	.0269	.300	.305	.1493	.0707	.1820	-.0329	98.0	29.87	41.7	1996.6
9.16	.193	|	1.082	1.458	.0849	1.2	1.202	.0255	14.79	.0499	.0264	.330	.305	.1029	.0706	.0849	.0018	98.3	29.96	41.8	2001.4
9.3	.20	|	.993	2.291	.1900	-5.0	2.704	-.2371	33.74	-.471	.0306	.303	.305	.1604	.0700	.1893	-.0166	123.7	37.70	45.0	2154.6
10.17	.233	|	.806	1.488	.1100	78.8	.3218	1.630	6.74	5.432	.0261	.246	.305	.0985	.0662	.0213	.1079	121.5	37.03	59.0	2824.9
10.83	.229	↓	.990	2.443	.1874	-4.8	2.960	-.2488	37.70	-.504	.0272	.302	.305	.1542	.0631	.1868	-.0157	116.5	35.51	58.5	2801.0
9.15	.192	.0556	.984	3.495	.3149	52.1	4.373	-.8416	30.97	-.9486	.0555	.300	.305	.2471	.0707	.3092	-.0595	98.0	29.87	41.7	1996.6
14.79	.347	.0050	1.041	----	.0163	-82.1	-----	-----	3.00	-2.847	.0048	.307	.295	.0590	-----	.0027	-.0161	180.5	55.02	128.3	6143.0
15.18	.359	.0050	1.000	----	.0206	-84.4	-----	-----	1.80	-2.447	.0077	.295	.295	.0853	-----	.0024	-.0205	188.0	57.30	138.2	6617.0
10.77	.228	.0182	1.072	1.099	.0519	5.0	.8142	-.0646	13.56	-.1711	.0178	.327	.305	.0698	.0635	.0517	-.0041	116.5	35.51	58.5	2801.0
9.15	.192	.0197	.905	1.194	.0724	72.9	.3013	.9788	6.67	3.451	.0209	.276	.305	.0844	.0707	.0213	.0692	98.0	29.87	41.7	1996.6
9.16	.193	.0197	1.082	1.255	.0630	-1.3	.8924	-.0198	14.50	-.0513	.0199	.330	.305	.0886	.0706	.0630	-.0014	98.3	29.96	41.8	2001.4
10.24	.233	.0197	.990	2.180	.1788	-7.8	2.685	-.3652	51.61	-9.977	.0188	.302	.305	.1439	.0660	.1772	-.0241	121.3	36.97	59.3	2839.3
8.34	.191	.0329	.993	1.914	.1531	-17.2	2.001	-.6197	24.16	-1.190	.0330	.303	.305	.1399	.0731	.1463	-.0453	99.1	30.20	39.6	1896.0